SEARCHES FOR NEW PHYSICS

Conveners: G.F. Giudice, M.L. Mangano, G. Ridolfi, and R. Rückl

Working group: S. Ambrosanio, S. Asai, G. Azuelos, H. Baer, A. Bartl, W. Bernreuther, M. Besançon, G. Bhattacharyya, M. Brhlik, L.M. Bryant, G. Burkart, M. Carena, R. Casalbuoni, P. Chankowski, D. Choudhury, A. Culatti, A. Deandrea, W. de Boer, G. Carlino, S. De Curtis, G. Degrassi, C. Dionisi, A. Djouadi, D. Dominici, H. Dreiner, H. Eberl, L. Favart, M. Felcini, F. Feruglio, H. Fraas, F. Franke, R. Gatto, S. Giagu, M. Grazzini, J.F. Grivaz, J.J. Hernandez, S. Katsanevas, S. Komamiya, S. Kraml, P. Le Coultre, S. Lola, W. Majerotto, A. Masiero T. Medcalf, B. Mele, G. Montagna, R. Munroe, S. Navas, F. Nessi-Tedaldi, O. Nicrosini, S. Orito, F. Piccinini, S. Pokorski, W. Porod, P. Rebecchi, F. Richard, S. Rigolin, S. Rosier-Lees, S. Shevchenko, V. Shoutko, A. Shvorob, L. Silvestrini, A. Sopczak, R. Tafirout, X. Tata, J. Toth A. Trombini, C. Vander Velde, R. van Kooten, A. Vicini, J.H. von Wimmersperg-Toeller, C. Wagner, K. Yoshimura.

Contents

1 Supersymmetry

1.1 Introduction

Supersymmetry (SUSY) [1, 2] represents the best motivated known extension of the Standard Model (SM). It offers an elegant solution to the naturalness problem of the Higgs sector [3], it is consistent with present experimental data, and it predicts new particles to be discovered in this generation of collider experiments. LEP2 has great potential for discovering SUSY, as a consistent solution of the naturalness problem suggests that some of the new weakly interacting particles are within the LEP2 energy range [4].

In the minimal SUSY model (MSSM), each SM particle has one SUSY partner. The partners of the gauge bosons (gauginos) have spin 1/2, the partners of fermions (sfermions) have spin 0 and the partners of the Higgs fields (higgsinos) have spin 1/2. The Higgs sector is enlarged to contain two complex weak doublets. After electroweak (EW) symmetry breaking, the partners of the Higgs and $SU_2 \times U_1$ gauge bosons mix, and the physical mass eigenstates are given by two Dirac fermions with one unit of electric charge (the charginos $\tilde{\chi}_i^\pm$, $i = 1, 2$ with $m_{\tilde{\chi}_1^\pm} < m_{\tilde{\chi}_2^\pm}$) and four neutral Majorana fermions (the neutralinos, $\tilde{\chi}_i^0$, $i = 1, ..., 4$ with $m_{\tilde{\chi}_i^0} < m_{\tilde{\chi}_j^0}$ if $i < j$). This sector is described by three parameters: the SU_2 gaugino mass M_2, the Higgsino mass μ, and $\tan\beta$, the ratio of the two Higgs vacuum expectation values (VEVs). The U_1 gaugino mass is given by the unification condition $M_1 = \frac{5}{3}\tan^2\theta_W M_2$, a relation valid in most GUT SUSY models. Relations between the three parameters M_2, μ, $\tan\beta$ and the masses and couplings of charginos and neutralinos can be found in ref. [2].

Each quark and lepton has two scalar partners, one for each chirality state. We will refer to these as left and right squarks ($\tilde{q}$) and sleptons ($\tilde{\ell}$). The scalar mass eigenstates are given by mixtures of these two left and right states. The squark and slepton mixing angles and masses are in general free parameters of the theory, and we will treat them as such. However, in sect. 1.8, we will analyze the more restricted case in which all squark and slepton masses are universal at the grand unification scale and then are evolved to low energies according to the renormalization group equations. This case, suggested by a certain class of supergravity theories, allows a simple comparison among the discovery potentials of different experimental searches, because all SUSY particle masses and interactions are described by only four free parameters.

The requirement of baryon and lepton number conservation in renormalizable interactions implies the existence of a discrete symmetry in the MSSM. Such symmetry, called R-parity, distinguishes between ordinary and SUSY particles and implies that: *i)* the SUSY particles can only be pair produced and *ii)* the lightest SUSY particle (LSP) is stable. An appealing feature of models with universal SUSY breaking terms at the GUT scale is that the neutralino turns out to be the LSP in almost all of the parameter space consistent with radiative EW symmetry breaking. This is welcome because from cosmological arguments on particle relic abundance [5] it follows that the LSP must be a neutral particle. In most of our analysis we will therefore

assume that the LSP is a neutralino, although we will also comment on the case in which the LSP is a sneutrino, the only other neutral SUSY particle in the MSSM.

Searches at LEP1 have ruled out charged SUSY particles lighter than about $m_Z/2$ [6]. For particular values of the SUSY parameters, the $\tilde{t}$ can decouple from the Z^0, and in this case the limit on the stop mass is slightly reduced [7, 8]. From measurements of the invisible Z^0 width, a sneutrino lighter than about $m_Z/2$ is also ruled out. The experimental limits on neutralinos [9] strongly depend on the SUSY parameters which determine their couplings to the Z^0. Tevatron bounds [10] on gluinos and squarks exclude the possibility of producing these particles at LEP2, with the notable exception of a light $\tilde{t}$. Information about the possible existence of light SUSY particles can also be extracted from global fits of EW observables, and it will be discussed in sect. 1.2.

In sects. 1.3–1.6 we present a study of the expected signals and detection efficiencies respectively for production of charginos, sleptons, stops, and neutralinos at LEP2. As alternatives to the MSSM, we will also consider two extensions which have some theoretical interest. In sect. 1.6.2 we discuss how neutralino searches are modified by the introduction of a new singlet superfield. Finally the rather different experimental signatures of SUSY in the presence of R-parity violation are studied in sect. 1.7.

1.2   Supersymmetry and R_b

The SM (and the MSSM with all superpartners heavy) is in excellent agreement with most of the electroweak measurements [11, 12, 13, 14, 15, 16] except for R_b and R_c [17]. The present experimental results, $R_b = 0.2219 \pm 0.0017$, $R_c = 0.1540 \pm 0.0074$, are respectively $+3.7\sigma$ and -2.5σ away from the SM predictions $R_b^{SM} = 0.2156$, $R_c^{SM} = 0.172$ (for $m_t = 180$ GeV) [11]. If R_c is fixed to its SM value, the fits give $R_b = 0.2205 \pm 0.0016$ [11].

In the MSSM it is possible to obtain larger R_b [18, 19, 20] without altering the rest of the EW observables [16]. Indeed, the latter are sensitive essentially only to additional sources of the custodial $SU_V(2)$ breaking in the "oblique" corrections, *i.e.* mainly to the left slepton and squark masses. The dependence on the right sfermion masses enters only through the left–right mixing. Since the breaking of the custodial $SU_V(2)$ in the gaugino and Higgs sectors is weak, the MSSM with heavy enough left sfermions does not significantly alter the SM predictions for those observables [15, 16]. The case of R_b is different. Its value can be larger than in the SM: for low $\tan\beta$ R_b receives important corrections from loops involving right stops and higgsino-like charginos. For large $\tan\beta$ loops involving the $CP-$odd Higgs contribute as well.

In fig. 1 we show the contours of constant R_b in the $(m_{\tilde{t}_1}, m_{\tilde{\chi}^\pm})$ plane for low $\tan\beta$ and in the $(M_A, m_{\tilde{\chi}^\pm})$ plane for large $\tan\beta$. For each point in the plane of fig. 1 the plotted R_b is the largest value obtainable by varying the remaining SUSY parameters under the the following assumptions [16]: *i)* the overall χ^2 in a fit to 14 electroweak observables is within $\Delta\chi^2 < 1$ from the best fit in that particular point; *ii)* the predicted $BR(b \to s\gamma)$ [21] is in the range
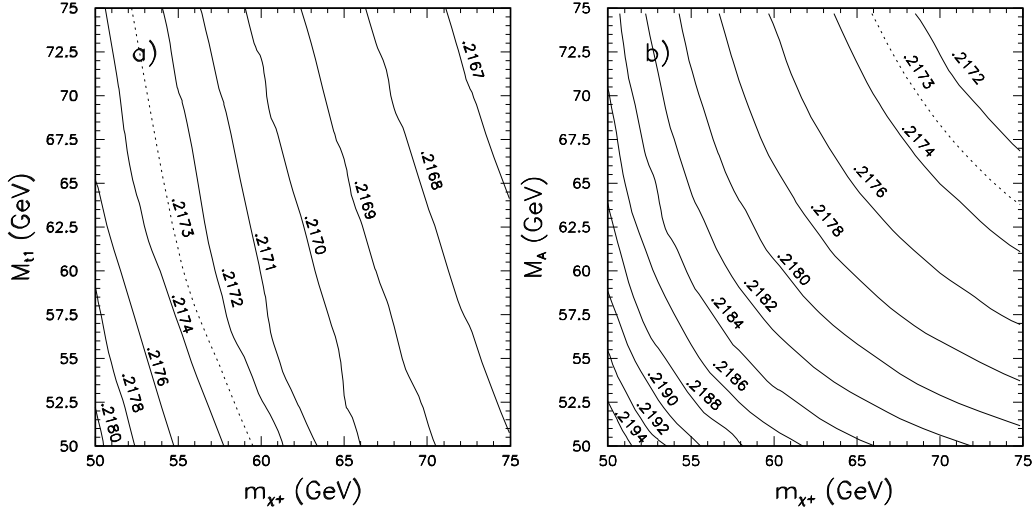
Figure 1: *Contours of constant R_b for $m_t = 180$ GeV a) in the chargino – lighter stop mass plane for $\tan\beta = 1.6$; b) in the chargino – CP−odd Higgs boson mass plane for large $\tan\beta = 50$.*

$(1 - 4) \times 10^{-4}$; *iii)* $BR(t \to bW) > 50\%$; *iv)* $\Gamma(Z^0 \to \chi_1^0\chi_1^0) < 4$ MeV; *v)* the Higgs mass is larger than 50 GeV.

Although with the constraints from LEP1 one cannot reach the central experimental value of R_b, supersymmetric corrections can significantly reduce the discrepancy [16]. For instance, for low $\tan\beta$ and $M_{\tilde{t}_1} = m_{\chi^+} = 50$ GeV one gets $R_b = 0.2182$ and for large $\tan\beta$ and $M_A = 55$ GeV, $m_{\chi^+} = 50$ GeV one gets $R_b = 0.2196$ and a significant improvement in the overall χ^2 w.r.t. the SM case. The supersymmetric R_b prediction remains within the 95% C.L. range $(R_b > 0.2173)$ in the region bounded by the dashed contours. The values of $\tan\beta$ chosen in fig. 1 are consistent with perturbative Yukawa couplings up to the Grand Unification scale and with constraints from $BR(b \to c\tau\nu)$ [22].

LEP1.5 data could push the lower limit for charginos up to $m_{\tilde{\chi}^\pm} > 65$ GeV provided that $m_{\tilde{\chi}^\pm} - m_{\tilde{\chi}_1^0} > 10$ GeV. Notice however that the regions of SUSY parameter space which provide the best R_b values do not satisfy this constraint. As in our fit we find very small mass splittings $m_{\tilde{\chi}^\pm} - m_{\tilde{\chi}_1^0}$ the chargino may well escape detection and therefore LEP1.5 measurements may not significantly restrict the SUSY corrections to R_b. However SUSY can bring the prediction for R_b within the 95% CL range from the data only if at least some SUSY particle is within the reach of LEP2. The region in parameter space selected by the best fits is interesting from the theoretical point of view [23, 24]. The hierarchy $|\mu| << M_2$ (i.e. higgsino–like lightest neutralino and chargino) is inconsistent with the mechanism of radiative electroweak symmetry breaking and universal boundary conditions for the scalar masses at the GUT scale However,
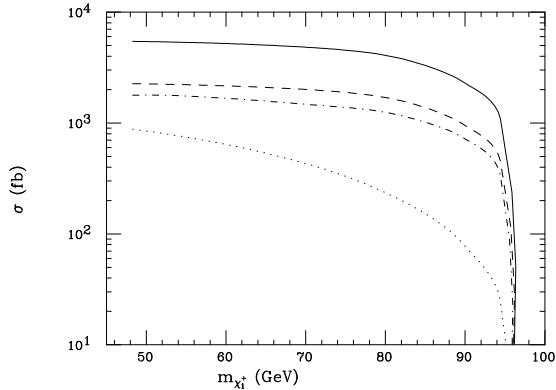
Figure 2: *Chargino production cross sections at LEP2, $\sqrt{s} = 190$ GeV, as a function of $m_{\tilde{\chi}_1^\pm}$. We show the ranges obtained by varying M_2, μ, $\tan\beta$ and $m_{\tilde{\nu}_e}$ throughout the parameter space, requiring $m_{\tilde{\nu}_e} > 45$ GeV. The solid and dotted lines correspond to the maximum and minimum production rates. The dashed (dash-dotted) line corresponds to the minimum cross section if $m_{\tilde{\nu}_e} = 2$ TeV ($m_{\tilde{\nu}_e} = 200$ GeV).*

it is predicted in models with certain pattern of non–universal boundary conditions [25].

1.3 Chargino

The MSSM contains two chargino mass eigenstates, $\tilde{\chi}_1^\pm$ and $\tilde{\chi}_2^\pm$. The lighter one, $\tilde{\chi}_1^\pm$, is a candidate for being the lightest SUSY charged particle. In e^+e^- collisions, charginos are pair produced via γ and Z exchange in the s-channel, and via $\tilde{\nu}_e$–exchange in the t-channel. This latter contribution is totally suppressed at LEP1. However at LEP2 energies, the destructive interference of the two contributions can lead to a considerable reduction of the production cross section if the $\tilde{\nu}_e$ is sufficiently light. In fig. 2 we present the minimum and maximum $\sigma(e^+e^- \to \chi_1^+ \chi_1^-)$ as a function of $m_{\tilde{\chi}_1^\pm}$, obtained by varying the SUSY parameters $\tan\beta$, $m_{\tilde{\nu}_e}$, M_2, and μ. As one can see, while the cross section is generally large, of the order of several pb, for special values of the above parameters it can be reduced to less than one pb, even away from the kinematic limit. Notice that the effects of destructive interference become less dramatic as soon as $m_{\tilde{\nu}_e} > 200$ GeV.

The main $\tilde{\chi}_1^\pm$ decay mode is expected to be:

$$\tilde{\chi}_1^\pm \to \tilde{\chi}_1^0 f \bar{f}' \tag{1.1}$$

with f and $\bar{f}'$ being fermions of the same weak isospin doublet and $\tilde{\chi}_1^0$ the lightest neutralino, which is assumed to be the lightest SUSY particle. The chargino decay can occur via virtual exchange of W, sfermions or charged Higgs boson. If H^+ and all sfermions are very massive ($m_{H^+}, m_{\tilde{f}} \gg m_W$), the BR are the same as those of the W. If the slepton masses are significantly

6

smaller than the squark masses and of the order of m_W, the $\tilde{\chi}_1^\pm$ leptonic BR are enhanced. Suppression of the hadronic modes due to phase space can also take place when the mass difference between the chargino and the lightest neutralino is small. Moreover, for some values of the SUSY parameters the second lightest neutralino, $\tilde{\chi}_2^0$, can be lighter than the lightest chargino and therefore the decay $\tilde{\chi}_1^\pm \to \tilde{\chi}_2^0 f\bar{f}'$ be possible. This can reduce the BR of decay mode (1.1) and give rise to cascade events with more leptons and more jets. The possible outcomes in terms of cross sections, decay modes and branching ratios as a function of the SUSY parameters have been extensively studied in the literature [26].

If $\tilde{\nu}$ or $\tilde{\ell}$ are lighter than the chargino, the decay modes $\tilde{\chi}_1^\pm \to \ell\tilde{\nu}_\ell$ or $\tilde{\chi}_1^\pm \to \tilde{\ell}\nu_\ell$ are accessible. The decays to lepton-sneutrino or slepton-neutrino would yield signals similar to those from slepton pair production and could be looked for in similar ways. As mentioned earlier, the region in which the chargino cross section is suppressed corresponds to a light sneutrino and a gaugino-like chargino. In this situation, the decay mode $\tilde{\chi}_1^\pm \to \ell\tilde{\nu}_\ell$ becomes dominant, see fig. 2. The efficiency for chargino detection is therefore improved and can compensate for the lower production cross section.

The experimental studies of the four LEP experiments that we present here [27] have only considered the three body decays in (1.1), so three kinds of events can be observed depending on whether the charginos decay to leptons or quarks: a pair of acoplanar leptons that may have different lepton flavour ($\ell\ell$ mode); a relatively isolated lepton with two hadronic jets and missing energy ($jj\ell$ mode) and hadronic events with missing energy ($4j$ mode). These modes may lead to different experimentally observed topologies. For example a $jj\ell$ event where the lepton is a τ that decays hadronically may look rather like a four-jet event than two jets plus a lepton.

In the Monte Carlo studies carried out by the LEP experiments, the BR of the $\tilde{\chi}_1^\pm$ have been assumed to be those of the W, so that the probability of the above modes are taken to be 10.3%, 43.5% and 46.0%, respectively.

The relevant backgrounds to this process are given in table 1. The most dangerous background is W^+W^- pair production due to the presence of missing energy and visible final states similar to those of the signal. Even though $\gamma\gamma$ events are very sensitive to the cuts used and should be a manageable background, care should be taken to have them well under control through a good knowledge of the apparatus. Indeed, the extremely high cross section of this kind of events makes it unfeasible to generate luminosities of simulated events large enough to match the number of expected real events. The experiments have used a *preselection* in order to discard at the generation level those events that would be in any case rejected after simulation. This procedure keeps only the tails of the distributions which may be a dangerous background of fake missing energy events. Cross-checks have been performed by the experiments to make sure that the different generators used to produce this background according to the various theoretical models (VDM, QPM and QCD) agree with data at LEP1 energies. The backgrounds have been generated using standard Monte Carlo programs [28, 29]. Chargino events were generated using SUSYGEN [30]. For a typical point in SUSY parameter space the

Type of event	Cross Section (pb)	
	$\sqrt{s} = 175$ GeV	$\sqrt{s} = 192$ GeV
$e^+e^- \rightarrow f\,\bar{f}\,(\gamma)$	164.9	128.1
$e^+e^- \rightarrow W^+W^-\,(\gamma)$	13.8	17.1
$e^+e^- \rightarrow Z^0 Z^0\,(\gamma)$	0.4	1.1
$e^+e^- \rightarrow W\,e\,\nu\,(\gamma)$	0.5	0.7
$e^+e^- \rightarrow Z^0\,e\,e\,(\gamma)$	2.7	2.9

Table 1: *Relevant backgrounds to chargino production and their cross sections at $\sqrt{s} =$ 175 and 192 GeV. The cross section for the $\gamma\gamma$ process is not given since it is highly dependent on the initial cuts used.*

L3 experiment has checked that using the Monte Carlo program DFGT [30], which properly takes into account spin-correlations, gives essentially the same detection efficiency.

1.3.1 Mode $jj\ell$

The $jj\ell$ mode has been studied with full simulation of the detector for several points of the SUSY parameter space by DELPHI, L3 and OPAL and with fast simulation by ALEPH.

The main features of the $jj\ell$ mode are the presence of an isolated lepton in a high multiplicity environment, a low hadronic mass, a high missing mass and high missing p_T. The initial selection of this mode is carried out with a cut in multiplicity and the identification of an isolated electron or muon (OPAL also includes a simplified τ identification by looking for 3 or 5 charged tracks in a 5° cone with an invariant mass smaller than 2 GeV).

The large $\gamma\gamma$ background is rejected demanding a high missing p_T (cuts range from 5 to 10 GeV), the absence of electromagnetic energy in the very forward-backward regions, and a missing momentum vector not pointing to the very forward-backward regions. For the non-$\gamma\gamma$ background, in particular due to W^+W^- production, a variety of cuts in visible mass, visible energy, missing mass, hadronic mass and invariant mass of the lepton and the unseen neutrino have been used by the four experiments. All these selection criteria take advantage of the fact that for W^+W^- events the missing mass is small (in fact with perfect resolution it would vanish since it is the neutrino mass), while the hadronic mass and the invariant mass of the lepton and unseen neutrino (as reconstructed from energy-momentum conservation) should be that of the W. On the other hand, in the chargino events the missing mass is large and the hadronic mass small due to the presence of the neutralino, while there is no particular reason why the "lepton–neutrino" invariant mass should peak at the W mass. Cuts in acoplanarity, acollinearity and maximum momentum of the isolated lepton are also included in the selection criteria of some
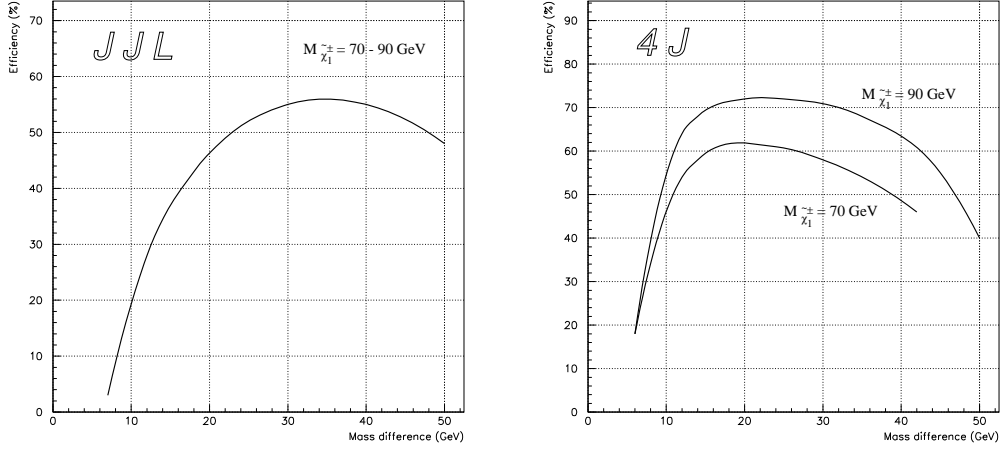
8

Figure 3: *Left: selection efficiency as a function of the chargino–neutralino mass difference in the $jj\ell$ mode for an average experiment. Right: same efficiency for the $4j$ mode. The two curves correspond to chargino masses of 70 and 90 GeV.*

of the experiments. The very same cuts devised for the W^+W^- background also reject the rest of non-$\gamma\gamma$ backgrounds, which are less important in terms of cross section, except for the $q\bar{q}\gamma$ background. At $\sqrt{s}= 190$ GeV all the four experiments are able to reduce the background to 50–100 fb. Around 30–50% of this background, depending on the experiment, is W^+W^-. The remaining background is mostly $q\bar{q}\gamma$ (20–30%) with contributions below the 10 fb level from the other processes.

Concerning the signal, the efficiency is in general only mildly dependent on the SUSY point considered. In fact, it is mostly dependent on the chargino and neutralino masses, and much less on their field composition. It is only when the chargino and neutralino are close in mass ($m_{\tilde{\chi}_1^\pm} - m_{\tilde{\chi}_1^0} < 10$ GeV) or the mass of the neutralino is very light ($m_{\tilde{\chi}_1^0} < 20$ GeV) that the efficiency starts to degrade (fig. 3, left). In the first case this is due to the decrease in multiplicity, visible energy and missing p_T; in the second, to the increase in visible energy and the decrease in missing mass, which makes these events more similar to the W^+W^- background. For the remaining chargino and neutralino mass values, the efficiency is quite stable. For the $jj\ell$ mode, in particular, the purely detector efficiencies for the electron and muon final states (*i.e.* excluding BR) range from 40 to 60% depending on the experiment. Taking into account the BR to the electron and muon final state (including those through the τ decay) the overall efficiency in this mode is in the 10 to 20% range, under the assumption that the chargino BR are equal to those of the W.

1.3.2 Mode $4j$

The $4j$ mode has been studied by DELPHI, L3 and OPAL for several points in the SUSY parameter space with full simulation of the detectors.

In this mode, high multiplicity and the absence of an isolated lepton are the first requirements. Again, the $\gamma\gamma$ background is rejected by means of cuts in minimum missing p_T and minimum acoplanarity. It is also required that only a limited amount of the total energy be present in the far forward-backward region and that the missing momentum vector does not point to this region. For the non-$\gamma\gamma$ background cuts have been applied on the minimum missing mass, on the maximum visible energy and on the maximum hadronic mass. As before, these cuts rely on the fact that the missing mass is low for the background and high for the signal, while the hadronic mass is around the center of mass energy for the background and low for the signal. Even though the background is in this case slightly higher than in the $jj\ell$ mode, it is nevertheless still in the 100–200 fb range. The experiments agree on the three main sources of background: W^+W^-, $q\bar{q}\,\gamma$ and $W\,e\,\nu$ events, but the percentage of each one changes from experiment to experiment, reflecting the different choices of cuts. It is worth noting that for this mode the $W\,e\,\nu$ process is a non-neglible source of background amounting to $\sim 30\%$ of the total.

The signal efficiency depends only very slightly on the chargino and neutralino masses unless we are close to the limit of a small neutralino mass (~ 20 GeV) or small chargino–neutralino mass difference. However, in this mode the search can be extended down to chargino–neutralino mass differences of the order of 5 GeV (see fig. 3, right). This lower mass difference is due to the higher multiplicity of the $4j$ mode, to the absence of the requirement of an isolated lepton, and to the smaller missing p_T needed to reject the $\gamma\gamma$ background. Another feature of this mode is that it recovers events missed in the $jj\ell$ mode. Indeed, some of the $jj\ell$ events that are lost during the $jj\ell$ selection are kept in the $4j$ selection. In case of discovery this "migration" might be a serious problem to compute branching ratios with the present selection criteria, but during the search stage it is a way of increasing the overall efficiency. The efficiency to select $4j$ events is, as in the preceding mode, in the 40–50% range. Additionally, around 15 to 20% of the $jj\ell$ events are classified also as $4j$. If we take into account also these events in our final sample, we obtain an "efficiency" of 60 to 70%.

1.3.3 Mode $\ell\ell$

The $\ell\ell$ mode has been studied with full simulation of the detector by DELPHI, L3 and OPAL for several points in the SUSY parameter space.

The $\ell\ell$ mode is characterized by two acoplanar leptons, low multiplicity, low visible energy, large missing mass and missing p_T. The final leptons might have different leptonic flavour, a feature that distinguishes this mode from the associated production of sleptons. The selection starts with a cut in multiplicity which is more or less stringent depending on whether the ex-
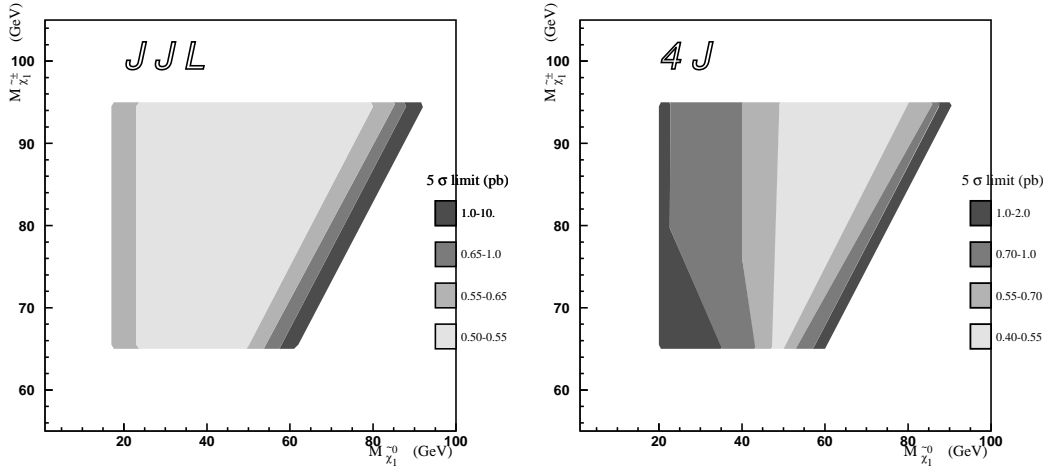
Figure 4: *Minimum signal cross sections required for 5-σ chargino discovery in the $(m_{\tilde{\chi}^{\pm}}, m_{\tilde{\chi}^0_1})$ plane, with 150 pb^{-1} integrated luminosity. The case of the $jj\ell$ mode (left) and of the $4j$ mode (right) are shown.*

periment additionally demands explicit lepton identification. Various ways of avoiding leptonic radiative return events have been used, all of them relying on some sort of restriction on the magnitude of the isolated electromagnetic energy in the event. Apart from this, cuts in the maximum energy in the far forward-backward cone are used to reject the $\gamma\gamma$ background.

W^+W^- events are mainly rejected by cuts in maximum visible energy, minimum missing mass or in the maximum momentum of the leptons. Apart from the acoplanarity, other variables in the transverse plane have also been used. In particular, cuts have been applied in "transverse thrust" and in the p_T–acoplanarity plane. The final background can be reduced to several tens of fb. The most serious background in this channel is W^+W^- production, which represents in all cases more than half the final background. The remaining background consists of radiative return and $Z\,e^+e^-$ events.

Concerning the signal, the average detector efficiency is in the 25–35% range. Again, this efficiency is rather stable throughout the SUSY parameter space, unless the neutralino is very light or very close in mass to the chargino. If we assume that the leptonic BR of the chargino is equal to that of the W, the overall efficiency in this mode is around 3%. In spite of this low efficiency, this mode is particularly important since its enhancement might indicate the possible presence of nearby sleptons.

11

1.3.4 Results

For $\sqrt{s}=$ 190 GeV, an integrated luminosity of 150 pb^{-1}, and assuming for the chargino the BR of the W, the LEP experiments are able to discover at the 5σ confidence level a chargino signal in the $jj\ell$ mode provided that its production cross section is above 0.5 to 0.8 pb, depending on the experiment. An integrated luminosity of 500 pb^{-1} would allow the exploration of the chargino signal in this same mode down to cross sections of 0.2 to 0.4 pb. Although the search can be carried out almost to the kinematical limit for both luminosities, when the chargino and neutralino are close in mass ($m_{\tilde{\chi}_1^\pm} - m_{\tilde{\chi}_1^0} < 10$ GeV) or the mass of the neutralino is very light ($m_{\tilde{\chi}_1^0} < 20$ GeV), the experimental efficiencies decrease very quickly. However, it is not excluded that more specialized selection criteria can be envisaged to recover, at least partially, these regions.

In the $4j$ mode, the minimum reachable cross section at $\sqrt{s}=$ 190 GeV to discover the chargino at the 5σ confidence level is in the 0.4–0.7 pb range, which can be reduced to 0.2–0.4 pb with an integrated luminosity of 500 pb^{-1}. In this mode, chargino–neutralino mass differences down to 5 GeV can be explored.

In fig. 4 we show the minimum cross-section at the 5σ confidence level for an integrated luminosity of 150 pb^{-1} for an average experiment in the chargino-neutralino mass plane, for the $jj\ell$ and the $4j$ mode.

In the $\ell\ell$ channel, the corresponding minimum cross section at $\sqrt{s}=$ 190 GeV is in the range 4–5 pb with 150 pb^{-1} and 2–3 pb with 500 pb^{-1}. The minimum chargino-neutralino mass difference is 10 GeV.

Combining the three modes and assuming an integrated luminosity of 150 pb^{-1}, the chargino search can go down to a minimum cross section of 0.3–0.5 pb depending on the experiment. This conclusion is reached under the assumption that the chargino BR are the same as those of the W. A variety of enhancements and suppressions of the leptonic and hadronic BR of the $\tilde{\chi}_1^\pm$ can take place depending on the relevant SUSY parameters, as was pointed out above. For these cases the above results can be properly rescaled.

1.4 Scalar Lepton Searches

Each SM charged lepton has two scalar partners, which will be called right and left sleptons. As mixings among different slepton states are assumed to be proportional to the corresponding Yukawa couplings, $\tilde{e}_{L,R}$ and $\tilde{\mu}_{L,R}$ are approximately mass eigenstates. On the other hand, a non-trivial mixing between the two $\tilde{\tau}$ states can be expected, especially for large $\tan\beta$. Smuons can be pair produced at LEP2 via Z and γ s-channel exchange. Their production cross section, corrected for ISR, is shown in fig. 5, as a function of $m_{\tilde{\mu}}$. Identical results hold for the $\tilde{\tau}$, in the limit of vanishing left-right mixing. In the case of the selectron, neutralino-exchange in the t-channel can also contribute to the production. Now the cross section is not uniquely
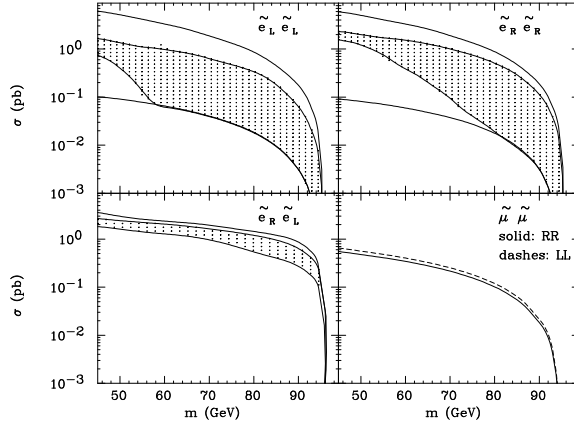
Figure 5: *Cross sections for the production of various slepton pairs at* 190 GeV, *as a function of the slepton mass. In the case of $\tilde{e}_L\tilde{e}_R$ production we assume $m_{\tilde{e}_L} = m_{\tilde{e}_R}$. ISR corrections are included throughout. For the selectron processes, the solid lines represent minimum and maximum rates obtained by varying M_2, μ and $\tan\beta$ in the range allowed by the LEP1 constraints. The shaded areas have the additional requirement $m_{\tilde{\chi}^\pm} > 95$ GeV. Notice that the minimum cross section for $\tilde{e}_L\tilde{e}_R$ is off scale when the $m_{\tilde{\chi}^\pm} > 95$ GeV requirement is not applied.*

determined by $m_{\tilde{e}}$, but it depends also on the neutralino parameters M_2, μ, and $\tan\beta$. As an effect of the t-channel exchange, the associated production of $\tilde{e}_L$ and $\tilde{e}_R$ is possible, even if the selectron mixing angle vanishes. Figure 5 shows the range of $\tilde{e}$-production cross sections in the three possible channels ($\tilde{e}_L\tilde{e}_L$, $\tilde{e}_R\tilde{e}_R$, $\tilde{e}_L\tilde{e}_R$). The minimum and maximum cross sections are obtained by varying the neutralino parameters within the range allowed by LEP1 constraints on charginos and neutralinos from the visible and invisible Z widths, consistently with the requirement that the neutralino is the LSP ($m_{\tilde{\chi}^0_1} < m_{\tilde{e}L,R}$). We also show the minimum and maximum cross sections obtained with the further requirement $m_{\tilde{\chi}^\pm} > 95$ GeV, expected to hold if the chargino search at LEP2 turns out to be unsuccessful. Because of the interference between s-channel and t-channel contributions, the $\tilde{e}$-production cross sections vary by more than an order of magnitude. Notice in particular that they could be significantly smaller than the $\tilde{\mu}$ cross section. Knowledge of (or constraints on) the parameters M_2, μ, and $\tan\beta$ from chargino and neutralino searches at LEP2 can be of great help to sharpen the predictions on the expected $\tilde{e}$ cross section.

Both left and right sleptons can decay into the corresponding charged lepton and a neutralino:

$$\tilde{\ell}^\pm \to \ell^\pm + \tilde{\chi}^0{}_i, \qquad i = 1, 2, 3, 4. \tag{1.2}$$

Left sleptons can also decay into the corresponding neutrino and a chargino:

$$\tilde{\ell}^\pm \to \nu_\ell + \tilde{\chi}^\pm{}_i, \qquad i = 1, 2. \tag{1.3}$$
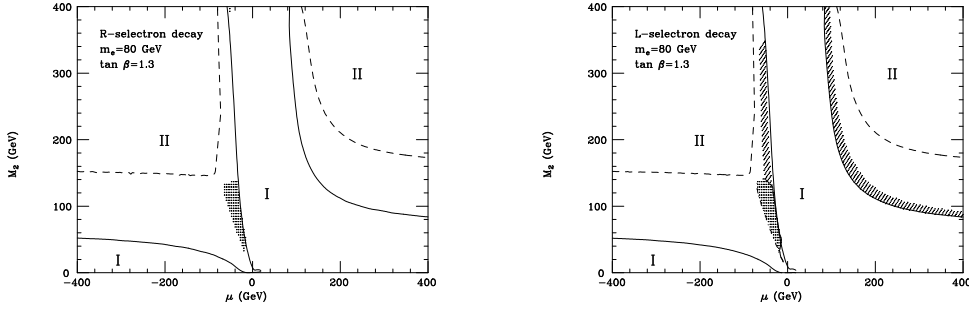
13

Figure 6: *Dominant slepton decay modes in the (M_2, μ) plane, for $m_{\tilde{\ell}} = 80$ GeV and $\tan\beta$=1.3. The regions labeled I are excluded by LEP1 data. The regions II do not satisfy $m_{\tilde{\ell}} > m_{\tilde{\chi}_1^0}$. The large unmarked regions correspond to $\tilde{\ell} \to \ell\tilde{\chi}_1^0$ being the dominant decay mode. In the dotted regions the dominant decay is $\tilde{\ell} \to \ell\tilde{\chi}_2^0$, while in the hatched area the dominant decay is $\tilde{\ell} \to \nu_\ell\tilde{\chi}_1^{\pm}$.*

If $m_{\tilde{\nu}_\ell} < m_{\tilde{\ell}} < m_{\chi^0}$ then $\tilde{\ell}$ will have only three-body decays. In our analysis we will not consider this possibility.

In the case of the right slepton, the decay mode $\tilde{\ell}_R^{\pm} \to \ell^{\pm} + \tilde{\chi}_1^0$ is always dominant, aside from a small region of parameters shown in fig. 6a where $\tilde{\ell}_R^{\pm} \to \ell^{\pm} + \tilde{\chi}_2^0$ is the main decay process. This region rapidly disappears as we increase $\tan\beta$. For left sleptons, the decay mode $\tilde{\ell}_L^{\pm} \to \nu_\ell + \tilde{\chi}_1^{\pm}$ can also become the dominant process in the region of parameters where the chargino is rather light, as illustrated in fig. 6b. Contrary to the case of $\tilde{\ell}_R$, the regions of the dominant $\tilde{\ell}_L$ decay modes do not significantly depend on $\tan\beta$.

The slepton decays into $\tilde{\chi}^{\pm}$ and $\tilde{\chi}_i^0$ $(i > 1)$ give rise to cascade processes, which may have very characteristic signatures [31]. In case of slepton discovery, these decay modes can give important information about the values of the relevant supersymmetric parameters.

The signature which was used in the studies that will now be presented is an acoplanar pair of charged leptons of the same flavour, accompanied by a large missing momentum. In order to investigate the detectability of selectrons at LEP2, a study was performed for the L3 experiment [32], relying on a detailed description of the detector in form of a fast simulation, with detector response and acceptance checked against data and against a full GEANT description. For the generation of selectron pairs, the BABY slepton generator described in ref. [33] was used, taking into account initial state radiation. In this generator, cascade decays are not included. Its use is nevertheless justified for the studied R-selectrons, which almost entirely decay to an electron and the lightest neutralino. The following background reactions have been considered:

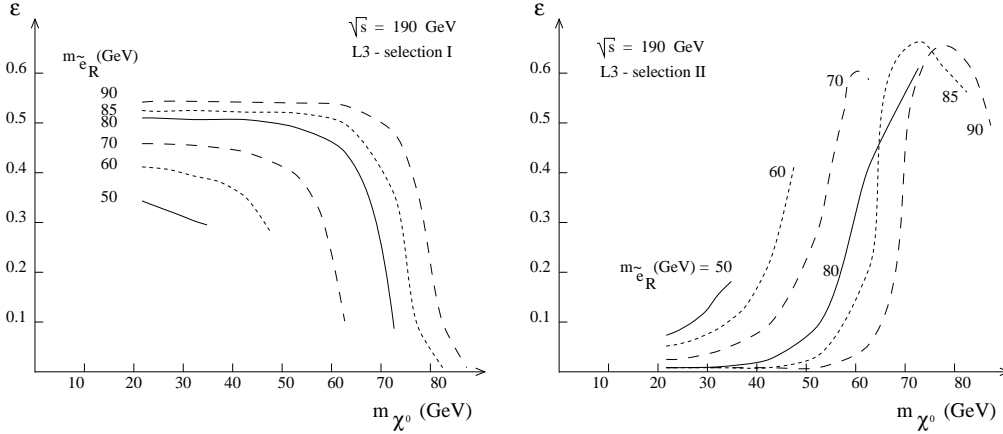$$e^+e^- \to l\bar{l}, W^+W^-, ZZ,$$

14

Figure 7: *Efficiency of the selection cuts I and II on selectron pairs of various masses, as a function of $m_{\tilde{\chi}_1^0}$.*

together with the photon interactions:

$$\gamma\gamma \to l\bar{l} \text{ and } e\gamma \to \nu W^{\mp}, e^{\mp}Z.$$

Looking for selectrons, only two electrons are expected in the detector, and some energy has to be missing, due to the neutralinos escaping detection. To suppress the background sources, while keeping a high signal efficiency, two sets of selections were used. For large values of the difference Δm between $m_{\tilde{e}}$ and $m_{\tilde{\chi}_1^0}$, an acoplanarity angle smaller than 130° and a total transverse momentum larger than 15 GeVare required (selection I). For the parameter space region where Δm is small, the acoplanarity angle was required to be below 160°, the total transverse momentum larger than 5 GeVand the missing energy in the event larger than 150 GeV (selection II).

The remaining background cross sections are 82 fb for selection I and 7.2 fb for selection II. The selection efficiencies for the signal are shown in fig. 7, for different selectron masses, as a function of the neutralino mass. For $m_{\tilde{e}} \geq 60$ GeV, they are larger than 40% for Δm > 15 GeV, and of the order of 60% for $5 <\Delta$m< 10 GeV, where the tight $\not{\!\!E}$ cut is most efficient.

Thus, the minimum signal cross sections needed for a 5σ statistical significance are, 143 fb (64 fb) in the region where selection I is applied, and 42 fb (19 fb) where selection II is used, for an integrated luminosity of 100 pb^{-1}(500 pb^{-1}). For $\mu = -200$, $\tan\beta = 4$ at $\sqrt{s} = 190$ GeV, the resulting discovery region in the ($m_{\tilde{e}}$, $m_{\tilde{\chi}_1^0}$) plane is shown in fig. 8a. The slight dip along the $m_{\tilde{\chi}_1^0}$ axis for high values of $m_{\tilde{e}}$ is due to the transition from one set of cuts to the other one. The lack of sensitivity observed in the region $m_{\tilde{e}} - m_{\tilde{\chi}_1^0} < 15$ GeV at low $m_{\tilde{e}}$ is mostly due to the particular choice of SUSY parameters and to the mass relations built into the BABY Monte-Carlo, which artificially restrict the possible values of the neutralino mass. The precise value of $m_{\tilde{e}} - m_{\tilde{\chi}_1^0}$ at which the detection efficiency will drop below the 10% level depends
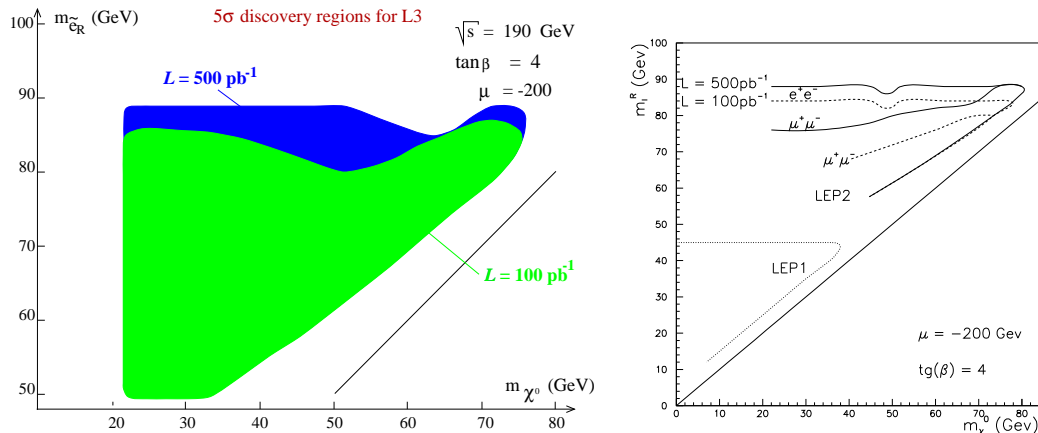
15

Figure 8: *Limits of detectabily of sleptons with* 5σ, *at 190* GeV, $\tan\beta = 4$ *and* $\mu = -200$ GeV, *for integrated luminosities of* $100pb^{-1}$ *and* $500pb^{-1}$, *in the plane* $m_{\tilde{\ell}} - m_{\tilde{\chi}_1^0}$, *(a) for* $\tilde{e}_R^+\tilde{e}_R^-$ *in the L3 detector at LEP II and (b) for right selectrons and smuons, in an ideal LEP detector.*

critically on the analysis cuts and on the accuracy of the detector simulation. Fig. 7 suggests that the L3 analysis could be sensitive to mass differences down to values of the order of $5-10$ GeV.

A similar exploratory study has been performed for selectron, smuon and stau pair production. In this preliminary study, the detector acceptance and performance have been crudely simulated by various cuts and by smearing the kinematical variables to take into account the measurement errors, see ref. [34]. The production of sleptons has been simulated using the generator SUSYGEN [30], taking into account ISR and cascade decays. The background processes have been simulated using PYTHIA [28]. In addition to the background processes generated in the preceeding analysis, the following reactions have been considered:

$$e^+e^- \to f\bar{f}, \nu\bar{\nu}Z \text{ and } \gamma\gamma \to f\bar{f}.$$

The selection cuts used for selectrons and smuons are very similar to those used in the L3 analysis. However three different sets are used instead of two, in order to try to suppress the dip observed in the contour of fig. 8a. Selection 3 is identical to selection II of L3 analysis. In selection 2, the missing energy cut is moved from 150 GeV to 130 GeV. In selection 1 the acoplanarity angle has to be smaller than 160°, the total transverse momentum larger than 15 GeVand the difference of longitudinal momentum between the negative and the positive lepton, has to be smaller than 40 GeV. As the τ can decay either leptonically or hadronically, the final state searched for is either 2 jets or a jet and a lepton. Two lepton final states, representing 13% of the total, would hardly be distinguished from smuon or selectron production. The total number of charged particles is limited to four, the acoplanarity angle must lie between 5° and 150°, the total transverse momentum between 15 and 29 GeVand the missing energy must be

16

larger than 150 GeV.

After applying the above selections, the cross section corresponding to the total remaining background, σ_b, is reduced to the values shown in table 2. The difference in background remaining for selectron production, compared with the L3 study, is due to the more realistic detector efficiencies used there.

Final state	e^+e^-	$\mu^+\mu^-$	$\tau^+\tau^-$
selection 1	115 fb	104 fb	
selection 2	23 fb	21 fb	55 fb
selection 3	11 fb	10 fb	

Table 2: Cross sections of remaining background, for e^+e^-, $\mu^+\mu^-$ and $\tau^+\tau^-$ final states.

The 5σ detectability ranges obtained after applying the above cuts on simulated signal events are shown in fig. 8b, assuming $\tan\beta = 4$ and $\mu = -200$ GeV. The results for selectrons and smuons are shown in the $m_{\tilde{\ell}} - m_{\tilde{\chi}_1^0}$ plane for $\mathcal{L} = 100\ pb^{-1}$ and $\mathcal{L} = 500\ pb^{-1}$. The agreement between selectron limits in both analyses brings some confidence in the cruder analysis of fig. 8b, which is the only one existing for smuons. With the above selection staus are not observed with 5σ at these luminosities, for this set of MSSM parameters. It is only possible in the most favourable case: $\mu < -50$ or $\mu > 300$ GeV and $\tan\beta \simeq 1$, at $\mathcal{L} = 500pb^{-1}$, for $m_{\tilde{\tau}} < 60$ GeV [35].

A further study involving a realistic simulation of the detector response has been performed at $\sqrt{s} = 190$ GeV for stau pairs in the OPAL detector [36]. It relies on a full detector simulation, with both background and signal generated with PYTHIA [28]; the stau mixing is neglected. A different set of cuts has been used than for the preliminary study above. They essentially differ by looser cuts on the transverse momentum and on the acoplanarity of the two jets in the final state: $p_T > 10$ GeV and $\theta > -3p_T(\text{GeV}) + 60^o$. This is compensated by a cut on detected gammas that must have less than 10 GeV. The missing energy cut is replaced by a cut on the two jet invariant mass that must be smaller than 50 GeV.

After these cuts, only 2 fb of background remain, allowing for a much lower value of the observed signal cross section, of the order of 12.5 fb, for $\mathcal{L} = 300pb^{-1}$, leading to a domain of detectability of stau pairs at $5\ \sigma$, shown in figure 9. The two contours correspond respectively to the case where the mass of the $\tilde{\tau}_R$ is much smaller than the mass of the $\tilde{\tau}_L$ and to the case where the two masses are degenerate. The above studies show that with 500 pb^{-1} selectron pairs could be detected at LEP2 with $5\ \sigma$ up to masses about 5 GeV below the kinematical limit, with $\Delta m > 10$ GeV. The reach could be significantly reduced if the SUSY parameters were such as to induce large destructive interference among the production diagrams. The domain of detectability for smuons is less model dependent, but limited to about 20 GeV below the kinematical limit. In the case of staus the reach is still more constrained, because of the

17
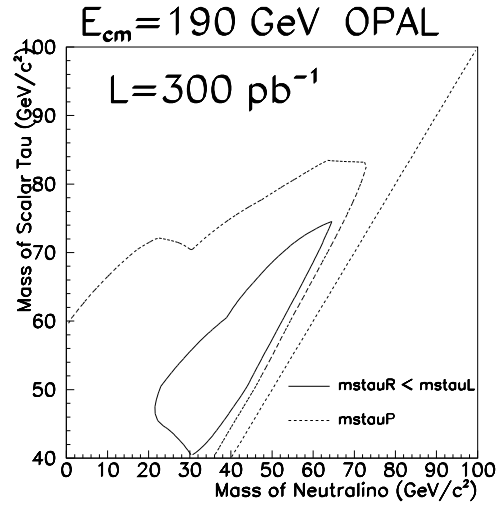
Figure 9: *OPAL's 5σ limits of detectability for stau pairs in the $m_{\tilde{\ell}} - m_{\tilde{\chi}_1^0}$ plane. $\sqrt{s} = 190$ GeV, for an integrated luminosity of 300 pb^{-1}.*

lower efficiency in the detection of the final state taus.

1.5 Stop and Sbottom

1.5.1 Phenomenological Aspects

The SUSY partners $\tilde{t}_L$ and $\tilde{t}_R$ of the top quark are expected to be mixed due to the large top Yukawa coupling. Therefore, the lighter mass eigenstate $\tilde{t}_1$ will most likely be the lightest squark and may even be the lightest visible SUSY particle. If $\tan\beta$ is large ($\tan\beta > 10$) also the sbottom $\tilde{b}_1$ can be rather light [37]. Thus, it may well be that $\tilde{t}_1$ or/and $\tilde{b}_1$ are within the reach of LEP2.

The mass matrix for the stops in the $(\tilde{t}_L, \tilde{t}_R)$ basis is given by [2]:

$$\mathcal{M}_{\tilde{t}}^2 = \begin{pmatrix} M_Q^2 + m_t^2 + m_Z^2 \cos 2\beta \left(T_{3t} - Q_t \sin^2\theta_W\right) & m_t\left(A_t - \mu\cot\beta\right) \\ m_t\left(A_t - \mu\cot\beta\right) & M_U^2 + m_t^2 + m_Z^2 \cos 2\beta\, Q_t \sin^2\theta_W \end{pmatrix} \quad (1.4)$$

where T_{3t} and Q_t are the third isospin-component and electric charge of the top quark, respectively. For the $\tilde{b}$ system analogous formulae hold with M_U^2 replaced by M_D^2 and with the off-diagonal element replaced by $m_b\left(A_b - \mu\tan\beta\right)$. The mass eigenstates are $\tilde{t}_1 = \cos\theta_{\tilde{t}}\,\tilde{t}_L + \sin\theta_{\tilde{t}}\,\tilde{t}_R$, $\tilde{t}_2 = -\sin\theta_{\tilde{t}}\,\tilde{t}_L + \cos\theta_{\tilde{t}}\,\tilde{t}_R$, and analogously for $\tilde{b}_{1,2}$. Thus, the experimental determination of the mass eigenvalues and the mixing angles provides information on the soft SUSY-breaking parameters M_Q, M_U, M_D, A_t, and A_b.

The reactions $e^+e^- \to \tilde{t}_1\bar{\tilde{t}}_1$ and $e^+e^- \to \tilde{b}_1\bar{\tilde{b}}_1$ proceed via s-channel γ and Z^0 exchange. The Z^0 couplings to $\tilde{q}_1\bar{\tilde{q}}_1$ are proportional $T_{3q}\cos^2\theta_{\tilde{q}} - Q_q\sin^2\theta_W$. In fig. 10 (a) and (b) we show the total cross sections for these processes at $\sqrt{s} = 175$ GeV and $\sqrt{s} = 192.5$ GeV as a function of $\cos\theta_{\tilde{t}}$ and $\cos\theta_{\tilde{b}}$ for several mass values of $\tilde{t}_1$ and $\tilde{b}_1$. Here we have included QCD radiative corrections and initial state radiation (ISR) [38, 39]. At $\sqrt{s} = 192.5$ GeV, for masses of 70 GeV the cross sections reach values of 0.7 pb and 0.55 pb for stop and sbottom production, respectively. There is a pronounced dependence on the mixing angle for $\cos\theta_{\tilde{t},\tilde{b}} \gtrsim 0.6$. Radiative corrections are impor-
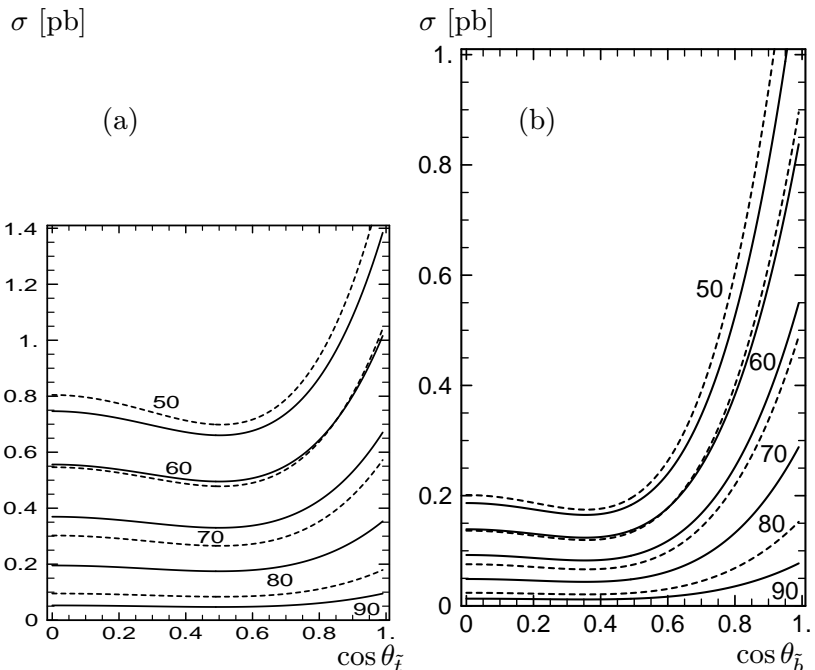
Figure 10: *Total cross section in pb at $\sqrt{s} = 175$ GeV (dashed lines) and $\sqrt{s} = 192.5$ GeV (solid lines) as a function of the mixing angle for squark masses of 50, 60, 70, 80, and 90 GeV, for (a) $e^+e^- \to \tilde{t}_1\bar{\tilde{t}}_1$ and (b) $e^+e^- \to \tilde{b}_1\bar{\tilde{b}}_1$.*

19

tant as can be seen in fig. 11, where we show the QCD and ISR corrected cross section together with the Born approximation for $e^+e^- \to \tilde{t}_1 \bar{\tilde{t}}_1$.

If $\tilde{t}_1$ is the lightest charged SUSY particle, it will decay with 100% branching ratio according to $\tilde{t}_1 \to c\,\tilde{\chi}_1^0$. If $m_{\tilde{t}_1} > m_{\tilde{\chi}_1^\pm} + m_b$, then the decay $\tilde{t}_1 \to b\,\tilde{\chi}_1^+$ has practically 100% branching ratio in the mass range of LEP2. In fig. 12 we show the domains of the $\tilde{t}_1$ decay modes in the $(M_2,\ \mu)$ plane for $m_{\tilde{t}_1} = 80$ GeV and $\tan\beta = 2$. There is a small strip where the decay $\tilde{t}_1 \to c\,\tilde{\chi}_2^0$ is also possible. The signature from the $c\,\tilde{\chi}_1^0$ decay is two jets and missing energy ($\not{E}$), whereas for $\tilde{t}_1 \to b\,\tilde{\chi}_1^+$ one has two b jets accompanied by two leptons + $\not{E}$, or lepton + jet + $\not{E}$, or two jets + $\not{E}$. In the case of $\tilde{t}_1 \to b\,\tilde{\chi}_1^+$ it will obviously be useful if the $\tilde{\chi}_1^+$ has already been observed and its main properties are known.

$\sigma\,(\tilde{t}_1 \bar{\tilde{t}}_1)$ [pb]

$\sqrt{s} = 192.5$ GeV
$\cos\theta_{\tilde{t}} = 0.4$

Figure 11: *Born approximation (- - -), QCD corrected (-.-), and QCD+ISR corrected (—) cross section for $e^+e^- \to \tilde{t}_1 \bar{\tilde{t}}_1$ as a function of $m_{\tilde{t}_1}$ for $\sqrt{s} = 192.5$ GeV and $\cos\theta_{\tilde{t}} = 0.4$.*

The lifetime of $\tilde{t}_1$ is expected to be larger than the hadronization scale [40]; thus $\tilde{t}_1$ hadronizes first into a colourless $(\tilde{t}_1\bar{q})$ bound state before decaying. This affects the spectrum and multiplicity of final state hadrons, as discussed in ref. [30]. The decay width for $\tilde{t}_1 \to b\,\tilde{\chi}_1^+$ becomes larger than 0.2 GeV for $m_{\tilde{t}_1} - m_{\tilde{\chi}_1^\pm} \gtrsim 25$ GeV and $\cos\theta_{\tilde{t}} > 0.9$.
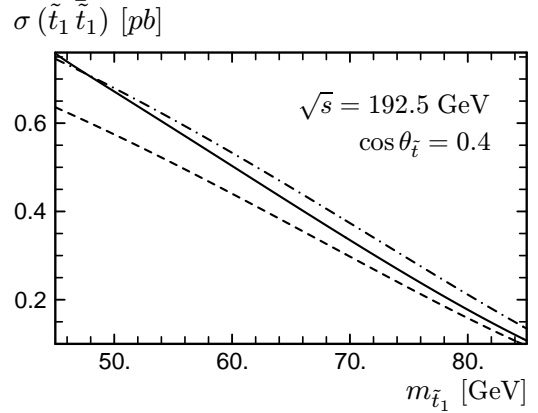

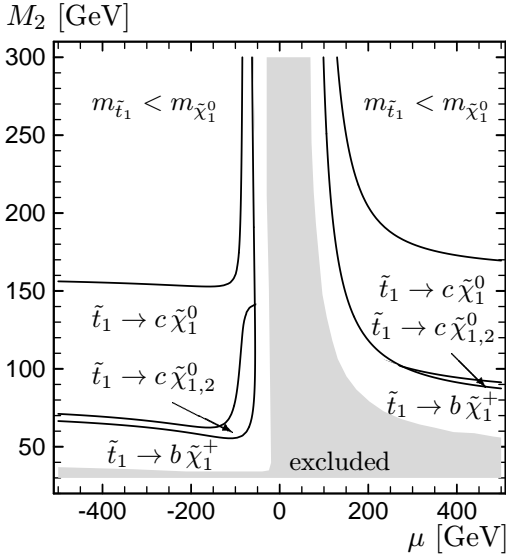Figure 12: *Parameter domains in the $(M_2,\ \mu)$ plane for the various $\tilde{t}_1$ decay modes, for $m_{\tilde{t}_1} = 80$ GeV and $\tan\beta = 2$. The grey area is excluded by LEP1.*
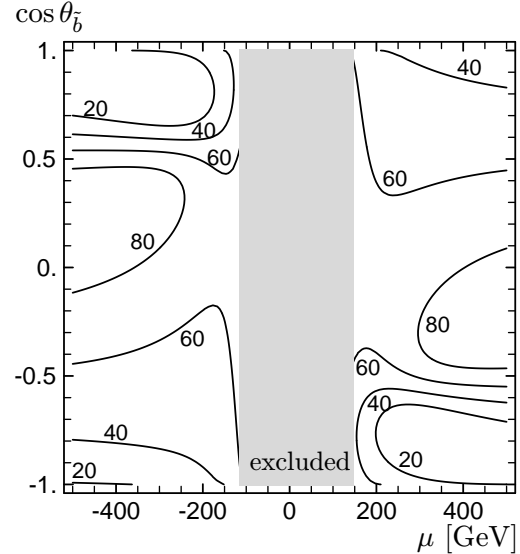

Figure 13: *Contour lines for the branching ratio (in %) of $\tilde{b}_1 \to b\,\tilde{\chi}_1^0$, for $m_{\tilde{b}_1} = 80$ GeV, $\tan\beta = 30$, and $M_2 = 60$ GeV. The grey area is excluded by LEP1.*
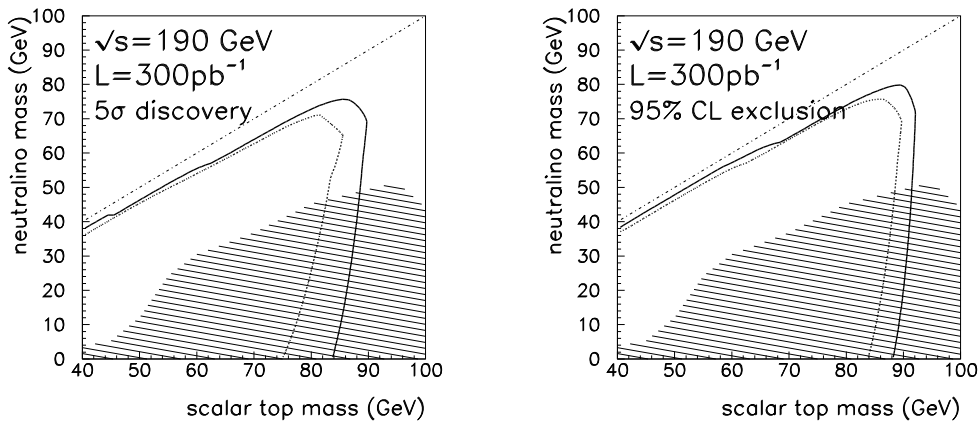
20

Figure 14: *5 σ discovery reach (left) and 95% CL limits (right) for the $\tilde{t}$ search at 190 GeV. The solid (dashed) lines correspond to maximal (minimal) coupling to the Z. The shaded area corresponds to the current 95% CL Tevatron limits [44].*

The main decay modes of the $\tilde{b}_1$ are $\tilde{b}_1 \rightarrow b\,\tilde{\chi}_1^0$ and $\tilde{b}_1 \rightarrow b\,\tilde{\chi}_2^0$, the second decay being possible in the parameter region approximately given by $M_2 < m_{\tilde{b}_1} - m_b$ or $|\mu| < m_{\tilde{b}_1} - m_b$. In fig. 13 we show the branching ratio for $\tilde{b}_1 \rightarrow b\,\tilde{\chi}_1^0$ as a function of $\cos\theta_{\tilde{b}}$ and μ for $m_{\tilde{b}_1} = 80$ GeV, $\tan\beta = 30$, and $M_2 = 60$ GeV. As can be seen, the decay $\tilde{b}_1 \rightarrow b\,\tilde{\chi}_2^0$ plays an important role for $|\cos\theta_{\tilde{b}}| > 0.5$. Moreover, there is a certain dependence on the sign of $\cos\theta_{\tilde{b}}$.

1.5.2 Search Strategy for Stop

A search for pair production of $\tilde{t}_1$ with $\tilde{t}_1$ decaying into $c\tilde{\chi}_1^0$ was made at LEP1 [7, 8]. The background situation at LEP2 is, however, more severe. DELPHI, L3 and OPAL have studied the search strategy for $\tilde{t}_1\bar{\tilde{t}}_1 \rightarrow c\tilde{\chi}_1^0\bar{c}\tilde{\chi}_1^0$ events. To determine the selection criteria, an integrated luminosity of 300-500 pb^{-1} was assumed at $\sqrt{s} = 190$ GeV. The $\tilde{t}_1\bar{\tilde{t}}_1$ event generators which are used for the three experiments are described in ref. [30]. The analyses were performed with realistic detector simulation. L3 [41] and OPAL [42] have applied cuts to the event shape and kinematical variables. DELPHI [43] has used a statistical method to set the cuts.

It is important to have a sensitivity for small values of the $\tilde{t}\tilde{\chi}_1^0$ mass difference (Δm) down to values of the order of 5 GeV, as it is difficult for the Tevatron experiments [44] to fully cover this region because of small missing p_T. The visible energy of $\tilde{t}_1\bar{\tilde{t}}_1$ events is small for small Δm, as the $\tilde{\chi}_1^0$'s carry a large fraction of energy, and the energy of particles form fragmentation in small. L3 and OPAL accept events with typical $E_{\mathrm{vis}} > 0.1\sqrt{s}$. In this case the main background is due to two photon processes. These background events can be reduced by a veto of the scattered electrons in the forward detectors (luminosity monitors). Typically, LEP detectors cover the forward region down to 25-50 mrad. The maximum p_T observed for two photon processes is determined by the forward coverage. Therefore the total transverse momentum of the events can be required to be larger than $\approx \theta_{\mathrm{min}}\sqrt{s}$, where θ_{min} is the minimum polar angle of the

Luminosity	coupling	5σ	95% C.L.	5σ	95% C.L.
Δm		20 GeV	20 GeV	10 GeV	10 GeV
75 pb^{-1}	full	83 GeV	87 GeV	79 GeV	83 GeV
	zero	73 GeV	82 GeV	67 GeV	77 GeV
150 pb^{-1}	full	87 GeV	90 GeV	83 GeV	87 GeV
	zero	81 GeV	86 GeV	77 GeV	82 GeV
500 pb^{-1}	full	91 GeV	91 GeV	88 GeV	91 GeV
	zero	88 GeV	90 GeV	84 GeV	88 GeV

Table 3: *The maximum $\tilde{t}_1$ mass for 5σ discovery and 95% C.L. exclusion at $\sqrt{s} = 190$ GeV as a function of the integrated luminosity. The numbers are for one typical LEP experiment for the two cases of the full and zero coupling of $\tilde{t}_1$ to the Z boson.*

coverage. The balance between the two photon background rejection and the signal efficiency determines the E_{vis} or p_T cuts.

For large Δm ($\gtrsim$ 20 GeV), the main background sources are $W^+W^- \to \ell\nu q\bar{q}'$ and $ZZ \to \nu\bar{\nu}q\bar{q}$ events. These events can be reduced by requiring the visible invariant mass of the events to be larger than $\approx$ 50 GeV. A cut against isolated leptons can be used to reject events with $W \to \ell\nu$ decays. The lower value of the visible energy cut can be tightened to eliminate the background from the two photon processes.

Since $\tilde{t}_1\bar{\tilde{t}}_1$ events are expected to have two narrow jets, the number of reconstructed jets is required to be two. The jet resolution parameter are optimized to have a good rejection of background and a good signal efficiency. This requirement reduces four jet events from W^+W^- or ZZ background as well as QCD multi-jet events. L3 used the JADE jet algorithm. OPAL used the Lund jet algorithm with the jet resolution parameter $d_{\text{join}} = (2.5 + 2E_{\text{vis}}/\sqrt{s})$ GeV. The E_{vis} dependence of the d_{join} parameter is needed for a good jet reconstruction over a wide range of $m_{\tilde{t}_1}$. Since the jet resolution parameter used for OPAL is tight, multi-jet events are effectively reduced and the other cuts can be loosened. Likewise, the L3 two-jet requirement is very efficient in removing multi-jet backgrounds. Another possibility to eliminate $q\bar{q}(\gamma)$ events or four jet events from W^+W^- or ZZ events is setting a cut on the maximum value of E_{vis}. To reduce the two jet $q\bar{q}$ background, the acoplanarity angle (ϕ_{acop}) cut is very powerful. The acoplanarity angle is defined to be 180° minus the opening angle between two jet momenta projected on to the plane pependicular to the beam axis. The events which have back-to-back topology in the plane perpendicular to the beam direction are reduced in this way. Therefore, $Z\gamma \to q\bar{q}\gamma$ events where the γ escapes into the beam pipe are also reduced. L3 has applied the cut $\phi_{\text{acop}} > 34°$, OPAL has taken $\phi_{\text{acop}} > 15°$ for $E_{\text{vis}} > 0.2\sqrt{s}$ and linearly increased the ϕ_{acop} cut value to 40° as E_{vis} decreased to $0.1\sqrt{s}$.

If the two jets are emitted close to the beam axis, the acoplanarity angle measurement

becomes poor. Therefore a cut $|\cos\theta_T| \lesssim 0.7$ is usually applied to the polar angle θ_T of event thrust axis. Events with a jet in the forward direction may also cause a large acoplanarity angle. The azimuthal angle of the forward jet cannot be measured with good precision because the particles belonging to the jet spread over a large azimuthal angle range. Events are rejected if one of the two jets points close to the beam axis. To further reduce $q\bar{q}\gamma$ events where the γ escapes into the beam pipe, L3 required the longitudinal momentum balance $|\Sigma p_z|/E_{\text{vis}} < 0.5$, where Σ runs over all the particles.

The detection efficiency of $\tilde{t}_1 \bar{\tilde{t}}_1$ events is about 25% for $m_{\tilde{t}_1} = 70$ GeV and $\Delta m = 20$ GeV, and large background rejection is maintained. For $\mathcal{L}=500$ pb^{-1} only 2–3 background events are expected. The efficiency increases gradually to 40% at $m_{\tilde{t}_1} = 85$ GeV with the same Δm. For $\Delta m = 10$ GeV, the efficiency is about 20% at $m_{\tilde{t}_1} = 70$ GeV, as the visible energy decreases. It goes down to a few % for $\Delta m = 5$ GeV.

DELPHI has chosen a very different approach. A statistical method is used to extract the signal from background. After a loose pre-selection of events, one applies a cut discriminating analysis *à la* Fisher with up to 31 kinematical and event shape variables: V_i $(i = 1, 2, ..., 31)$. The discrimination function F is calculated as a linear combination of the variables: $F = a_0 + \sum_{i=1}^{31} a_i V_i$, where the coefficients a_i are optimized to have the best separation between signal and background. The discovery potential is evaluated from the number of expected signal to background events after having applied a cut on F, which is optimized in order to maximize the discovery potential. The analysis is repeated for different masses of $\tilde{t}_1$ and $\tilde{\chi}_1^0$ as well as for different $\sqrt{s}$ (175 GeV and 190 GeV) focusing on small Δm.

The five sigma discovery and 95% CL exclusion regions in the $m_{\tilde{t}_1}$-$m_{\tilde{\chi}_1^0}$ plane, which can be reached by a typical LEP analysis at $\sqrt{s} = 190$ GeV, are shown in fig. 14. The shaded area corresponds to the region currently excluded at the 95% CL by searches at the Tevatron collider [44]. The minimum luminosity needed for five sigma discovery and for 95% C.L. exclusion in the cases of $\Delta m = 10$ and 20 GeV are given in table 3.

No effort has been made so far to study $\tilde{t}_1$ identification. For this purpose it is important to identify the charm quark in the $\tilde{t}_1 \to c\tilde{\chi}_1^0$ decay. After applying appropriate selection cuts, the enhancement of the soft $\pi^\pm$ from D^* decay, the reconstructed D or D^* mass peak and the leptons from charm semileptonic decays can be studied to identify the charm quark. A direct mass reconstruction is not straightforward due to the large missing mass arising form the two neutralinos. In the case of $\tilde{t}_1 \to b\tilde{\chi}_1^+$ the visible energy is larger than in $\tilde{t}_1 \to c\tilde{\chi}_1^0$, and b-tagging can be used to enhance the signal. If one of the $\tilde{\chi}_1^\pm$'s decays into $\tilde{\chi}_1^0 \ell^+\nu$, an isolated lepton is expected in the event. These leptons are softer than those from W^+W^- or ZZ events. If the $\tilde{\chi}_1^\pm$ is lighter than $\tilde{t}_1$, it is most likely that it will be discovered first. The information of the $\tilde{\chi}_1^\pm$ characteristics can be used to identify $\tilde{t}_1$ by the decay into $b\tilde{\chi}_1^+$.

DELPHI has studied the decay $\tilde{t}_1 \to b\tilde{\chi}_1^+$ using the same method as described above. Additionally, the vertex information has been used to enhance events with b-quark. The experimental reach for $m_{\tilde{t}_1}$ is 85 GeV at $\sqrt{s} = 190$ GeV, with a luminosity of 300 pb^{-1}. Moreover, DELPHI has studied $\tilde{b}_1$ search when $\tilde{b}_1$ decays into $b\tilde{\chi}_1^0$. The discovery potential for $\tilde{b}_1$ is similar
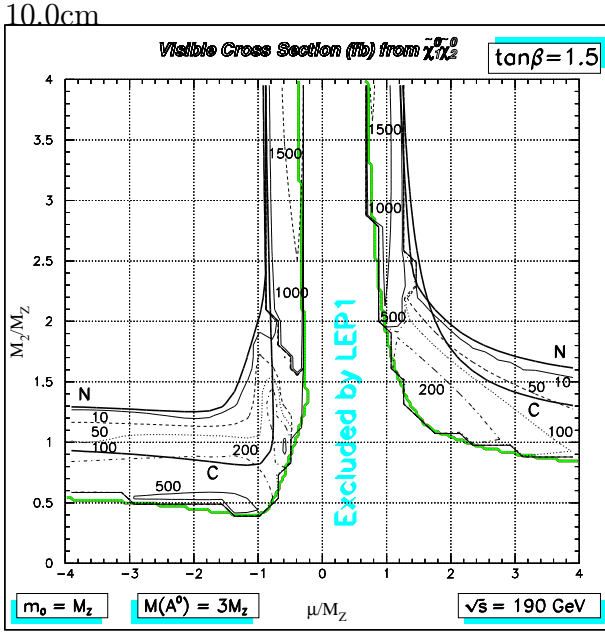
10.0cm

Figure 15: *Contour lines for the cross section (fb) of $e^+e^- \to \tilde{\chi}_1^0 \tilde{\chi}_2^0 \to$ visible, in the (μ, M_2) plane, for $\tan\beta = 1.5$, $m_0 = M_Z$, $M_{A^0} = 3M_Z$. The central empty region is excluded by LEP1 data. The bold lines represent the kinematical limits for $e^+e^- \to \tilde{\chi}_1^0 \tilde{\chi}_2^0$ ('N') and $e^+e^- \to \tilde{\chi}_1^+ \tilde{\chi}_1^-$ ('C') at LEP2 ($\sqrt{s} = 190$ GeV).*

to that of the $\tilde{t}_1 \to c\tilde{\chi}_1^0$.

1.6   Neutralinos

The most promising neutralino production process at LEP2 is the production of a lightest plus a next-to-lightest neutralino, $e^+e^- \to \tilde{\chi}_1^0 \tilde{\chi}_2^0$. In fact, most of the times the $\tilde{\chi}_2^0$ decays in some visible final state (plus a $\tilde{\chi}_1^0$) while the lightest neutralino goes undetected, producing a large imbalance in the final state momentum and missing mass.

A thorough study of the production rates at LEP2 for the process $e^+e^- \to \tilde{\chi}_1^0 \tilde{\chi}_2^0$, which takes into account all the possible signatures that can derive from the different $\tilde{\chi}_2^0$ decays, has been performed as a function of the SUSY parameters μ, M_2, $\tan\beta$, and the common scalar mass m_0 [45]. The $\tilde{\chi}_2^0$ can decay into a $\tilde{\chi}_1^0$ plus: $\ell^+\ell^-$, $\nu_\ell\bar{\nu}_\ell$, $q\bar{q}$, $\ell^+\ell'^-\nu_\ell\bar{\nu}_{\ell'}$, $\ell^\pm\nu_\ell q\bar{q}'$, $q_1\bar{q}_1'q_2\bar{q}_2'$ (the last three arising from cascade decays through a light chargino) or a photon. Possible decays into a light Higgs boson have also been included. A typical scenario is shown in fig. 15, where the rates for all visible $\tilde{\chi}_2^0$ final states are included. At LEP2, one finds that:

a) In regions where $\tilde{\chi}_1^0$ and $\tilde{\chi}_2^0$ are mostly higgsino-like (*i.e.* for $|\mu| \lesssim M_Z$ and $M_2 \gtrsim 1.5M_Z$) production rates are large (more than 1 pb) and comparable to the chargino rates.
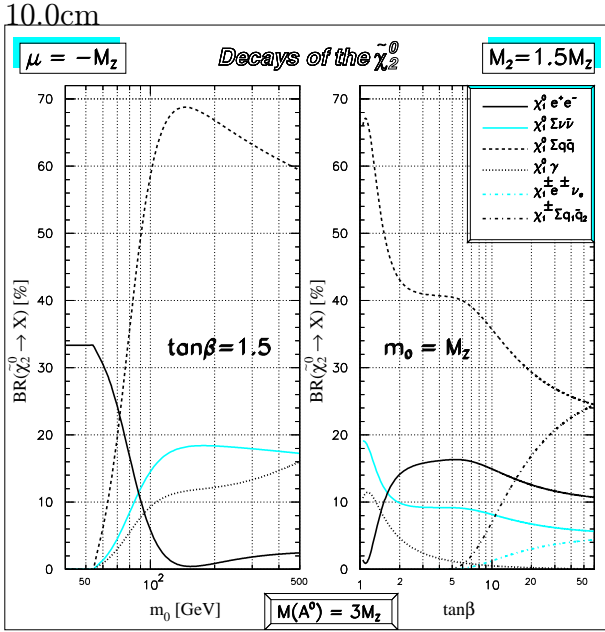
10.0cm

Figure 16: *B.R.'s of all $\tilde{\chi}_2^0$ decay channels for $\mu = m_Z$, $M_2 = 1.5 m_Z$, $m_{A^0} = 3 m_Z$ as functions of m_0 (with $\tan\beta = 1.5$) and of $\tan\beta$ (with $m_0 = m_Z$).*

b) In regions where $\tilde{\chi}_1^0$ and $\tilde{\chi}_2^0$ have non-negligible gaugino components (*i.e.* for $|\mu| \gtrsim M_Z$), the kinematical reach (marked by 'N' in fig. 15) of the reaction $e^+ e^- \to \tilde{\chi}_1^0 \tilde{\chi}_2^0$ in the (μ, M_2) plane is larger than the one relative to the light chargino-pair production (marked by 'C' in fig. 15).

c) For $|\mu| \gtrsim M_Z$, the neutralino production rates are much lower than the chargino rates (mainly due to the absence of the γ-exchange channel for neutral particles) and critically dependent on selectron masses. For $\tilde{e}$ close to the LEP2 reach (*i.e.* $m_0 \simeq M_Z$ GeV), cross sections up to about 0.5 pb can be reached outside the regions excluded by LEP1, and up to 0.2 pb in the area not covered by chargino searches at LEP2.

Hence, neutralino production provides a remarkable additional tool to explore the SUSY parameter space in the regions covered by light-chargino pair production and beyond. Comparative chargino/neutralino studies in more constrained SUSY models, which assume radiative breaking of the EW symmetry, are reported in sect. 1.8.

A detailed analysis of the $\tilde{\chi}_2^0$ partial decay widths and branching ratios is necessary to establish the actual fraction of detectable events from $e^+ e^- \to \tilde{\chi}_1^0 \tilde{\chi}_2^0$. The results of this analysis [46], are critically dependent on the physical $\tilde{\chi}_2^0$ compositions and on the assumed s-fermion spectrum of the theory. An example is given in fig. 16, where the m_0 and $\tan\beta$ dependence of the $\tilde{\chi}_2^0$ branching ratios for all possible decays is shown for a typical scenario of interest for LEP2 searches, *i.e.*, $\mu = -m_Z$ and $M_2 = 1.5 m_Z$.

25
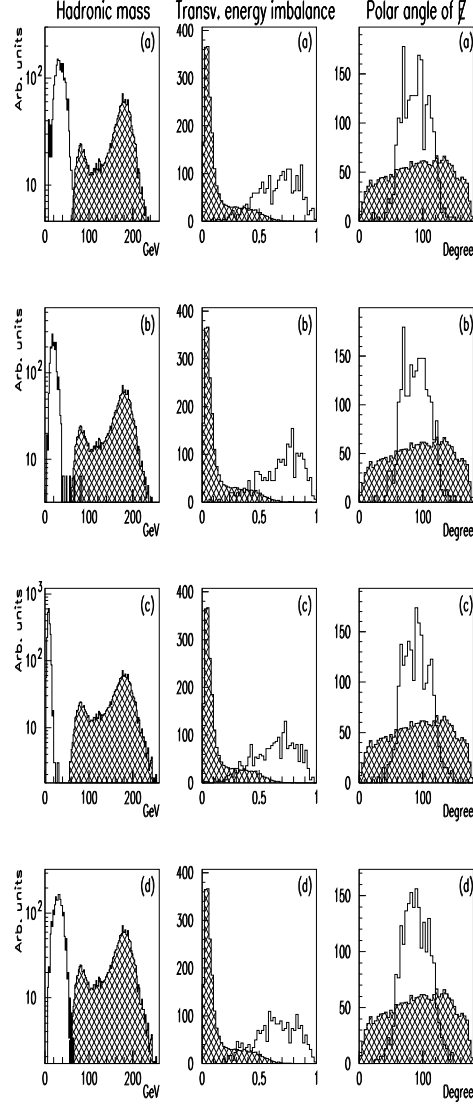
Figure 17: *Distributions of the most discriminating variables for the signal from $e^+e^- \to \tilde{\chi}_1^0 \tilde{\chi}_2^0 \to$ jets + missing momentum for cases (a), (b), (c) and (d) corresponding respectively to $(m_{\tilde{\chi}_1^0}, m_{\tilde{\chi}_2^0}) = (49.7, 107)$, (51.5, 85.2), (73.7, 89.8) and (56, 108.2) GeV. The distributions for signal (empty histogram) and the sum of the backgrounds from standard physics processes (hatched histogram) are normalized to the same integral.*

As already discussed in this report, a critical parameter for the detection of the neutralino and chargino production is the mass splitting between the decaying particle and the lightest neutralino. In the parameter region where M_2 is much larger than both μ and m_W, the lightest chargino and two lightest neutralinos are mainly higgsino-like and are nearly mass degenerate. However the mass difference $m_{\tilde{\chi}_2^0} - m_{\tilde{\chi}_1^0}$ is about twice as large as $m_{\tilde{\chi}^\pm} - m_{\tilde{\chi}_1^0}$ [47]. This is approximately true even after radiative corrections are included [48]. Since, in the case of higgsino-like neutralinos, the cross section for the process $e^+e^- \to \tilde{\chi}_1^0\tilde{\chi}_2^0$ is large (of the order of a pb), neutralino searches are very useful in studying a parameter region where chargino identification can be problematic [47]. Notice also that the higgsino-like region ($M_2 \gg \mu, m_W$) is favoured by the present R_b measurements at LEP1, as discussed in sect. 1.2.

Another neutralino channel that could be of interest for LEP2 is the radiative single-photon process $e^+e^- \to \tilde{\chi}_1^0\tilde{\chi}_1^0\gamma$, where a hard, large-angle photon accompanies the invisible $\tilde{\chi}_1^0$ pair. After applying typical experimental cuts on the photon, optimized for background suppression, (i.e., $p_\gamma^T/E_{beam} > 0.065$, $|\cos\theta_\gamma| < 0.95$, $E_\gamma/E_{beam} < 0.5$), one finds rates up to 40 fb in the gaugino regions, for moderate $\tilde{e}$ masses [49]. Unfortunately, the corresponding rate of the main background process, $e^+e^- \to \gamma\nu_\ell\bar{\nu}_\ell$, is about 900 fb and makes the radiative neutralino production very hard to isolate.

1.6.1 Search Strategy for Neutralinos

We have investigated the possibility of detecting a signal from the $\tilde{\chi}_1^0\tilde{\chi}_2^0$ associate production with the L3 experiment at $\sqrt{s} = 190$ GeV [50]. We have studied detection efficiencies and background rejection for the four points A, B, C, D of the MSSM, discussed in ref. [45], corresponding to the parameter region not covered by chargino searches, for which $(m_{\tilde{\chi}_1^0}, m_{\tilde{\chi}_2^0}) =$ (49.7, 107), (51.5, 85.2), (73.7, 89.8) and (56, 108.2) GeV.

The signal of $\tilde{\chi}_1^0\tilde{\chi}_2^0$ associate production, with $\tilde{\chi}_2^0 \to \tilde{\chi}_1^0 + q\bar{q}$ or $\ell^+\ell^-$ decay, is a pair of acoplanar jets or leptons and missing momentum from the two undetected $\tilde{\chi}_1^0$'s. Since the branching ratio of the $\tilde{\chi}_2^0$ in the hadronic or leptonic mode depends on the values of the parameters, we have studied separately the detection efficiencies and background rejections for the two modes.

We consider as background the known physics processes which can produce events with acoplanar jets or leptons + missing momentum. They are (in parenthesis the total cross section) $e^+e^- \to q\bar{q}\gamma$ (94 pb), WW (18 pb), $We\nu$ (0.92 pb), ZZ (1.1 pb), Zee (3.2 pb) and $ee \to ee\gamma\gamma \to f\bar{f}ee$ (3000 pb). The $ee \to ee\gamma\gamma \to f\bar{f}ee$ process, hereafter called the $\gamma\gamma$ process, despite the very large cross section, gives a negligible contribution to the total background, after the cuts which we describe in the following.

The signal events were generated with SUSYGEN [30], while the backgrounds were generated with PYTHIA. The events were then passed through the standard simulation and reconstruction of the L3 detector.

In the hadronic events, we require at least 4 tracks and 10 calorimetric clusters. Hadronic jets are reconstructed from the calorimetric clusters with the JADE algorithm, using y_{cut}=0.02. In order to reduce the background from WW (ZZ) with an isolated high momentum lepton in the final state, we require that there are no isolated electrons or muons with momentum higher than 20 GeV. In addition we require that there is no energy deposited in the very forward detectors. This cut reduces mainly $\gamma\gamma$ and Zee events, where one or both of the electrons are emitted in the very forward direction, and they can either hit the forward detectors or go undetected in the beam pipe. To reduce events with particles escaping in the beam pipe (from $qq(\gamma)$, Zee, $\gamma\gamma$), we require that the longitudinal imbalance be less than 40% of the total visible energy in the event. Exploiting the fact that the acoplanarity (defined as the complementary of the angular difference in the transverse plane among the two highest energy jets) is typically small for the background and large for the signal, we require the acoplanarity to be larger than 40°.

After the above cuts the most discriminating quantities are: (i) the hadronic mass, which is usually large for most of the backgrounds and small for the signal; (ii) the transverse imbalance, usually smaller in the background than in the signal; (iii) the polar angle of the missing momentum. The distributions of the most discriminating variables for the neutralino signals analyzed and the sum of the backgrounds are shown in fig. 17.

The requirement that the hadronic mass be between 5 and 50 GeV, the transverse imbalance above 40% of the total visible energy, and the polar angle of the missing momentum point between 20° and 160°, reduces the detected background cross section to 16 fb while the signal detection efficiencies is around 40% , almost independently of $m_{\tilde{\chi}_2^0}$ and $m_{\tilde{\chi}_1^0}$. It should be noted that, in the four cases analyzed, the $m_{\tilde{\chi}_2^0} - m_{\tilde{\chi}_1^0}$ mass difference is always above 15 GeV, so detection efficiency is not problematic as it is in the low mass difference region (see sect. 1.3).

Similar cuts to those applied in the hadronic channel are used in the leptonic channel, where two isolated electrons or muons are required. Cuts on the total energy, the longitudinal and transverse imbalance, the angle of the missing momentum, the acoplanarity and the mass of the lepton pairs allow to reduce the detected background cross sections to 25 fb and 20 fb for acoplanar electron and muon events, respectively. The detection efficiency is 40% and 30% for electrons and muons, respectively, almost independently of the neutralino masses and for mass differences above 15 GeV.

We conclude that 300 (100) pb^{-1} allow to detect a $\tilde{\chi}_2^0\tilde{\chi}_1^0$ signal in regions of the parameter space were the signal production cross section is above $\sim$ 100 (200) fb, for a $m_{\tilde{\chi}_2^0} - m_{\tilde{\chi}_1^0} > 15$ GeV.

1.6.2 Neutralinos in the NMSSM

The Next-to-Minimal SUSY Standard Model (NMSSM) is a simple extension of the MSSM, obtained by adding a singlet superfield and by allowing only cubic superpotential couplings [51].
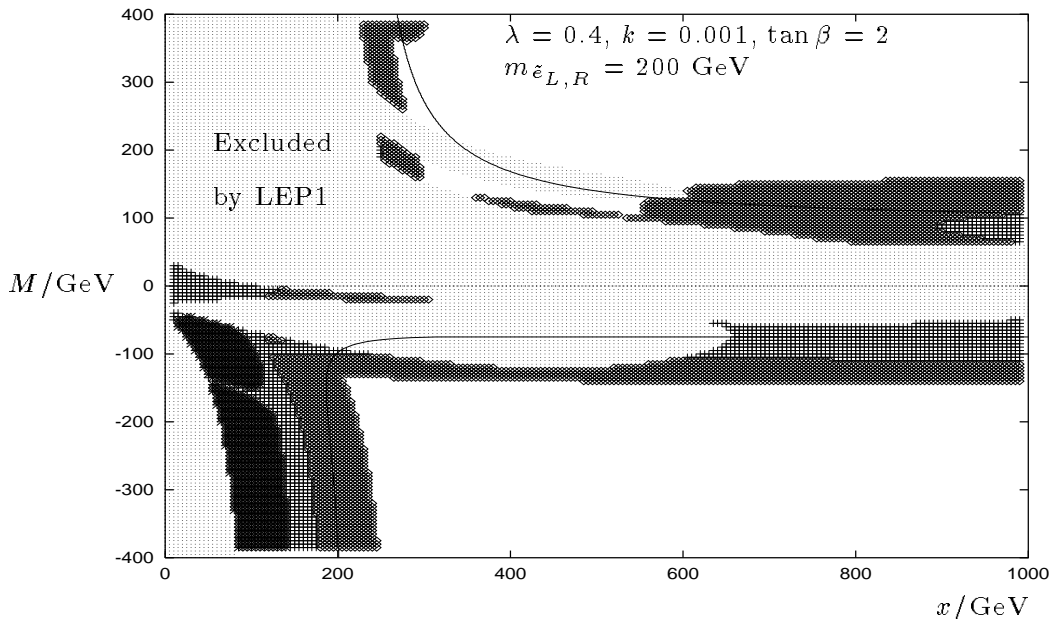
Figure 18: *Accessible parameter space at LEP2 ($\sqrt{s} = 190$ GeV). The different shadings denote regions where the $\tilde{\chi}_2^0$ production cross section is larger than 500, 200, and 100 fb (from dark to light). The contour line for $m_{\tilde{\chi}^\pm} = 95$ GeV is also shown.*

It contains five neutralinos with mass eigenstates and mixings determined by the singlet vacuum expectation value x and the couplings λ and k in the superpotential, in addition to the MSSM parameters M_1, M_2, and $\tan\beta$. Neutralino and Higgs sectors are strongly correlated in the NMSSM. In scenarios with light singlet-like neutralinos there often exist also light Higgs bosons with masses below the MSSM bounds. Contrary to the MSSM, the experimental data do not exclude very light or even massless neutralinos and Higgs bosons [52].

Fundamental differences between the NMSSM and the MSSM scenarios may occur when the neutralinos accessible at LEP2 have significant singlet components. Since the singlet superfield with zero hypercharge does not couple to (s)fermions and gauge bosons, neutralino pair production just differs because of the neutralino mixing.

For a typical NMSSM scenario, fig. 18 shows the areas of the parameter space not excluded by LEP1, where at least one production channel with a visible neutralino reaches a cross section above 100, 200 or 500 fb. In most of this region the lightest neutralino is singlet-like. A NMSSM scenario could be tested even for parameter regions beyond the kinematical limit for chargino production, *e.g.* in the large x domain. Here the lightest neutralino (assumed to be the LSP) is very light (≈ 10 GeV) while the visible next-to-lightest neutralino is produced at LEP2 and may be distinguished from the MSSM by its decay modes, as discussed below. On the other hand,
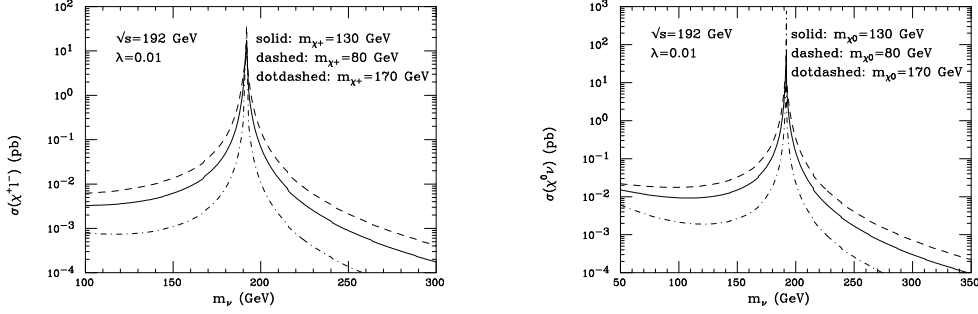
29

Figure 19: *Production cross section for $(\nu \tilde{\chi}_1^0)$ (a) and $(\ell^\mp \tilde{\chi}^\pm)$ (b) fianl states produced via R-parity violating s-channel $\tilde{\nu}_e$ exchange.*

there exists a region in fig. 18, where a chargino and a neutralino in a corresponding MSSM scenario with $\mu = \lambda x$ can be found, but for which in the NMSSM all light neutralinos have singlet components large enough to suppress their production at LEP2. In general, however, LEP2 considerably extends the parameter space which can be probed. In particular, small x values ($x \gtrsim 80$ GeV) can be excluded independently of the concrete NMSSM scenario if no neutralino is found. On the other hand, one cannot expect a stronger lower bound on the neutralino mass.

In order to estimate the prospects for identifying a NMSSM neutralino and distinguishing between NMSSM and MSSM, an analysis of the dominant decay channels of the produced neutralinos is essential. Compared to the MSSM, the decay of the next-to-lightest neutralino into a Higgs boson plus the LSP and the loop decay into a photon and the LSP is enhanced in typical NMSSM scenarios [53]. This happens because the singlet neutralino does not couple to the gauge sector, but only to the Higgs sector for $\lambda \neq 0$. Generally, the decay into a Higgs boson becomes dominant if kinematically allowed. Then, depending on the parameters of the Higgs sector, the Higgs may decay dominantly into b-quark pairs, but also into two invisible LSPs. If the next-to-lightest neutralino cannot decay into a Higgs boson, three-body decays with a fermion pair and the loop decay with a photon in the final state become comparable. In typical NMSSM scenarios as in fig. 18 the latter dominates for large x-values and vice versa. A detailed simulation study of these possibilities has not yet been performed.

In conclusion, it may be possible to distinguish a NMSSM neutralino from the minimal model at LEP2 if the LSP is mainly a singlet and the next-to-lightest neutralino is pair produced at the available center-of-mass energy. However unfavourable neutralino mixings may also prevent the discovery of a NMSSM neutralino at LEP2.

30

1.7 R-Parity Violation

The SUSY extension of the SM can contain the following renormalizable terms in the superpotential [2] beyond those present in the MSSM:

$$\lambda_{ijk} L_i L_j \bar{E}_k + \lambda'_{ijk} L_i Q_j \bar{D}_k + \lambda''_{ijk} \bar{U}_i \bar{D}_j \bar{D}_k. \tag{1.5}$$

Here Q_i, $\bar{U}_i$, $\bar{D}_i$, L_i and $\bar{E}_i$ ($i = 1, 2, 3$) denote the three generation quark and lepton superfields. These terms are allowed by gauge symmetry but forbidden by R-parity conservation, with $R = (-1)^{2S+3B+L}$ (S, B and L representing spin, baryon and lepton number). The interactions in eq. (1.5) lead in general to unacceptable rates for proton decay. However, if only a subset of these terms were allowed, *e.g.* by imposing some discrete symmetries, the proton can be stable but the superymmetric experimental signatures would be dramatically different. Examples of such discrete symmetries are baryon parity, lepton parity [54] or family symmetries [55]. In this section we study the phenomenology of including R-parity violating interactions. In this analysis it is assumed that (i) for each process considered, no more than one of the 45 coupling constants in eq. (1.5) is non-vanishing and (ii) the LSP is the lightest neutralino. The phenomenology of SUSY searches then changes in two important aspects.
(1) The LSP decays in the detector if any of the couplings in eq. (1.5) satisfies [56]

$$\lambda > 8 \times 10^{-6} \sqrt{\gamma_L} \left(m_{\tilde{f}}/150 \, \text{GeV} \right)^2 (45 \, \text{GeV}/M_{LSP})^{5/2}, \tag{1.6}$$

where γ_L is the Lorentz boost and $m_{\tilde{f}}$ is the relevant sfermion mass.
(2) At LEP200 single resonant sneutrino production can occur via the operators $L_1 L_{2,3} \bar{E}_1$.

$$e^+ e^- \to \tilde{\nu}^*_{2,3} \to (\nu \chi^0_1), (e^{\pm} \chi^{\mp}_1) \tag{1.7}$$

The resulting two sets of signals are discussed below.

MSSM-Production followed by LSP Decay. The MSSM production mechanisms are unaltered by the operators of eq. (1.5). However, the final state now includes the decay of the LSP, provided eq. (1.6) is satisfied. Thus the pair production of the two lightest neutralinos leads to a visible signal. For LEP2 and LEP140 this has been discussed in detail in ref. [57]. Furthermore, the full LSP decay as described in ref. [58] is included in SUSYGEN [30]. It should be clear that if the LEP2 energy is above *any* SUSY particle pair threshold, and no LSP decay is detected, then *all* the R-parity violating couplings in eq. (1.5) can be excluded down to the value given by eq. (1.6).

Resonant Sneutrino Production. The operator $L_1 L_{2,3} \bar{E}_1$ offers the unique possibility of resonant sneutrino ($\tilde{\nu}_e$) production. The BR($\tilde{\nu}_{2,3} \to e^+ e^-$) is strongly constrained by present bounds [59] on the coupling constants of eq. (1.5). Thus the sneutrino typically decays via a gaugino to an R-parity odd final state: $\tilde{\nu}_{2,3} \to \nu_{2,3} \tilde{\chi}^0_1$ or $\ell^-_{2,3} \tilde{\chi}^+_1$. The decay widths are given in ref. [59]. Explicitly the amplitude squared for the chargino production (1.7) is given by:

$$|\mathcal{M}|^2 (e^+ e^- \to \chi^-_1 \ell^+_{2,3}) \;\; = \;\; g^2 \lambda^2 |V_{11}|^2 \left(\frac{s(M^2_{\chi^-} - s)}{|R(s)|^2} + \frac{t(M^2_{\chi^-} - t)}{|D(t)|^2} - \mathcal{R} \frac{I(s,t,u)}{R(s)D(t)} \right) \tag{1.8}$$

where $R(s) = s - m_{\tilde{\nu}}^2 + i\Gamma_{\tilde{\nu}} m_{\tilde{\nu}}$, $D(t) = t - m_{\tilde{\nu}}^2$, and $I(s,t,u) = s(M_{\chi^-} - s) - u(M_{\chi^-} - u) + t(M_{\chi^-} - t)$. Here, $|V_{11}|^2 < 1$ is the gaugino fraction in the final state chargino, and $t = (p(e^-) - p(\chi))^2$. The cross sections are plotted in fig. 19 as functions of $m_{\tilde{\nu}_e}$ for $\sqrt{s} = 190$ GeV and $\lambda = 0.01$.

The $\tilde{\chi}_1^0$ will decay to $e^+ e^- \nu$ or $e^\pm e_{2,3}^\mp \nu$. The signal consists of two charged leptons typically in the same hemisphere and a large amount of missing p_T. The chargino can either decay directly via an R-parity violating coupling or it can decay to $\tilde{\chi}_1^0$. The amplitudes squared for the R-parity violating $(L_1 L_2 \bar{E}_1)$ decay $\chi^-(k) \to e^-(p_1)\mu^-(p_2)e^+(p_3)$ is given by $(s = (k+p_1)^2$, $t = (k - p_2)^2)$

$$|\mathcal{M}|_{\not{R}_p}^2 = g^2 \lambda^2 |V_{11}|^2 \left(\frac{s(s - M_\chi^2)}{|R(s)|^2} + \frac{t(t - M_\chi^2)}{|D(t)|^2} + \mathcal{R}e \frac{I(s,t,u)}{R(s)D(t)} \right) . \tag{1.9}$$

The branching fraction depends strongly on the size of λ and on the kinematical suppression due to the $\tilde{\chi}_1^0$ mass. In both cases the signal contains four charged leptons which should be clearly visible. Thus the chargino production is preferable to the LSP production. Since the cross sections are comparable, it is the main signal for R-parity violation.

1.8 Multi-mode Search for Minimal Supergravity at LEP2

We summarize in this section prospects for detecting SUSY at LEP2 assuming the paradigm case of the minimal supergravity (SUGRA) model. We assume gauge coupling unification and radiative EW symmetry breaking, along with universal soft SUSY-breaking terms at a GUT scale M_X taken to be equal to the scale at which the $U(1)$ and $SU(2)$ gauge couplings unify. The model parameters are thus m_0, the universal scalar mass, $m_{1/2}$, the universal gaugino mass, A_0, the universal trilinear term, $\tan\beta$, the ratio of Higgs field VEVs, and the sign of the SUSY conserving Higgsino mixing term μ. Along with m_t, these parameters suffice to determine the weak-scale sparticle masses and mixings, which in turn allow all sparticle and Higgs boson production cross sections and decay modes to be calculated. This allows to delineate the regions of parameter space accessible to searches at LEP2 and to distinguish the different SUSY signals from one another. It also allows to compare the potential of LEP2 with that of the Tevatron Main Injector $p\bar{p}$ collider, which is expected to begin collecting data around 1999.

The cross sections and decay modes have been embedded into the event generator ISAJET [60], [30]. All allowed SUSY and Higgs boson production mechanisms for the sampled points in SUGRA parameter space have then been generated, and compared against SM backgrounds such as $\tau\bar{\tau}$, WW and ZZ production. The latter two were calculated with complete spin correlations using the HELAS [61] package. Further details and results may be found in ref. [31], along with references to related studies.

In fig. 20, we show regions of the m_0 vs. $m_{1/2}$ plane explorable at LEP2 given $\sqrt{s} = 190$ GeV, and $\int \mathcal{L}dt = 500$ pb^{-1}. In all frames, we take $A_0 = 0$. In a), we take $\tan\beta = 2$, $\mu < 0$, while in b) we take $\tan\beta = 2$ with $\mu > 0$. In c), we take $\tan\beta = 10$, $\mu < 0$ and in d) we take $\tan\beta = 10$, $\mu > 0$. The regions denoted by TH are excluded by the theoretical constraints built into the model, such as the requirement of radiative EW symmetry breaking. The region labelled EX
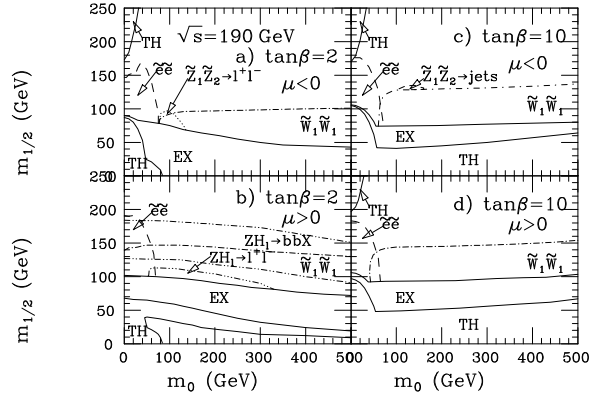
Figure 20: *Regions of the minimal supergravity parameter space explorable at LEP2 with $\sqrt{s} = 190$ GeV.*
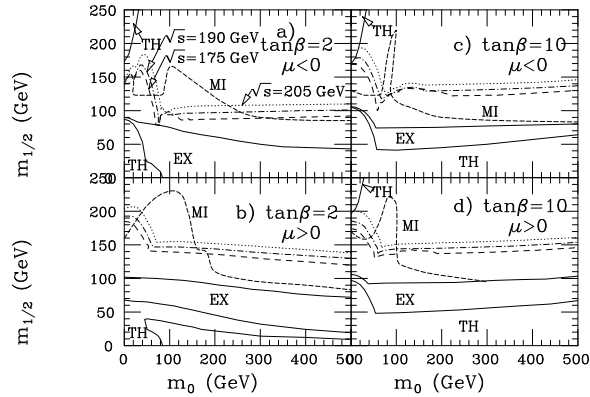

Figure 21: *Cumulative reach of various LEP2 options (and Tevatron MI) for SUSY particles (excluding Higgs bosons).*

is excluded by experimental constraints. We have implemented various cuts designed to select signal from SM background, and to separate SUSY processes from one another. In the lower left regions, $\tilde{e}\bar{\tilde{e}} \rightarrow e^+e^- + E\!\!\!\!/$ signals ought to be probed, whereas in the lower $m_{1/2}$ regions, chargino signals should be detectable via mixed leptonic/hadronic signatures. In addition, some small regions are noted where $\tilde{\chi}_1^0\tilde{\chi}_2^0$ can be seen via dilepton or jet signatures. If in fact a $\tilde{\chi}_1^0\tilde{\chi}_2^0$ signal is seen, then it may be best to run LEP2 around $\sqrt{s} = 150$ GeV, to eliminate backgrounds from WW and possibly Zh production; then the tiny $\tilde{\chi}_1^0\tilde{\chi}_2^0$ signal may be more easily examined in a relatively background free environment.

Higgs boson masses are correlated with the rest of the sparticle mass spectrum, and Zh production can be seen in significant regions of the $\tan\beta = 2$ frames. h is somewhat heavier in the $\tan\beta = 10$ frames, and so energies in excess of $\sqrt{s} = 190$ GeV will be needed in this case to see it.

In fig. 21, we show the cumulative reach of various LEP2 upgrade options for SUSY particles (excluding Higgs bosons), for $\sqrt{s} = 175$ GeV and $\int \mathcal{L}dt = 500$ pb^{-1} (dashed), $\sqrt{s} = 190$ GeV and $\int \mathcal{L}dt = 300$ pb^{-1} (dot-dashed), and $\sqrt{s} = 205$ GeV and $\int \mathcal{L}dt = 300$ pb^{-1} (dotted). Also shown for comparison is the combined reach of Tevatron Main Injector era experiments ($\sqrt{s} = 2$ TeV and $\int \mathcal{L}dt = 1000$ pb^{-1}) (dashed curve labelled by MI). We see regions of parameter space accessible to LEP2 that the MI cannot explore, and regions of parameter space open to MI that LEP2 cannot explore (except possibly via Higgs searches). These plots emphasize the complementarity between the two colliders.

In addition, in ref. [31] one can find a study of the regions of parameter space explorable via 3ℓ+jets and clean 4ℓ signatures ($\ell = e$ or μ). Such events arise from $\tilde{e}_L\tilde{e}_R$, $\tilde{\chi}_2^0\tilde{\chi}_2^0$, $\tilde{\nu}_e\bar{\tilde{\nu}}_e$ production with various cascade decays. These reactions generally occur within subsets of the regions of parameter space already delineated in fig. 20, and so give no additional reach for SUSY, in the constrained SUGRA model under consideration. The detection of such events is nonetheless important since it could serve to test the details of the underlying model. Also ref. [31] contains the corresponding regions of parameter space accessible at LEP2 via search for the lightest SUSY Higgs boson h. These regions can extend deep into parameter space; however, over a wide range of parameters, the SUSY h would be very difficult to distinguish from a SM Higgs boson.

2   New Fermions

2.1   Introduction

In this chapter we concentrate on the LEP2 potential for discovering new fermions (elementary or composite) other than those predicted by the MSSM. New quarks and leptons may arise in a class of theories with quark-lepton unification [62, 63] or in those that endeavour to answer questions about fermion masses and family replication [64, 62]. It is plausible that the symmetry

structure of the theory may protect their masses to be comparable to the Fermi scale, and indeed certain theoretical arguments [65] do indicate this to be true in a wide class of models. Excited fermions, on the other hand, are natural corollaries of models where the SM fermions themselves are composite particles rather than being elementary ones [66]. The mass gap is determined by the compositeness scale, and, for a not too large value of the latter, may be bridged by the LEP2 energy. In either case, then, looking for new fermions provides a probe of possible new physics beyond the SM.

2.2   New Elementary Fermions

These may be subdivided into two categories :

- sequential, *i.e.* with gauge quantum numbers identical to the SM fermions [64], or,

- exotic [62, 67] *i.e.* all those fermions that have no analog in the SM. Popular examples are provided by

  - mirror fermions which have chiral properties exactly opposite to those of the SM fermions;

  - vector fermions, whose left- and right-handed components have identical gauge quantum numbers; and

  - singlet neutrinos, which have no coupling with the SM gauge sector except through mixing, and consequently are the hardest to detect.

Since the SM gauge interactions of these new fermions are determined (apart from mixing effects) by their quantum numbers, some of the strongest bounds can be inferred from the absence of unexpected decay channels of the Z^0 at LEP. Thus, for all such fermions other than singlet neutrinos, we have $m_f \gtrsim 45$ GeV. At the Tevatron, though, stronger bounds (~ 85 GeV) can be imposed on new quarks, provided they decay within the detectors [6, 68]. These bounds are likely to improve with the new data. As lepton production at the Tevatron proceeds mainly through Drell-Yan-like processes or through gauge boson fusion, the corresponding bounds are expected to be somewhat weaker. However, such an analysis has not yet been reported in the literature. LEP data, along with other low-energy measurements can also be used to place strong bounds on the possible mixings that the new fermions may have with the SM particles [69]. Certain indirect bounds can also be placed from precision EW measurements at LEP as well as from some other low energy observables [70]. For example, the LEP bounds on the oblique parameter S (equivalently ϵ_3) restricts the number of additional chiral generations to be at most one.
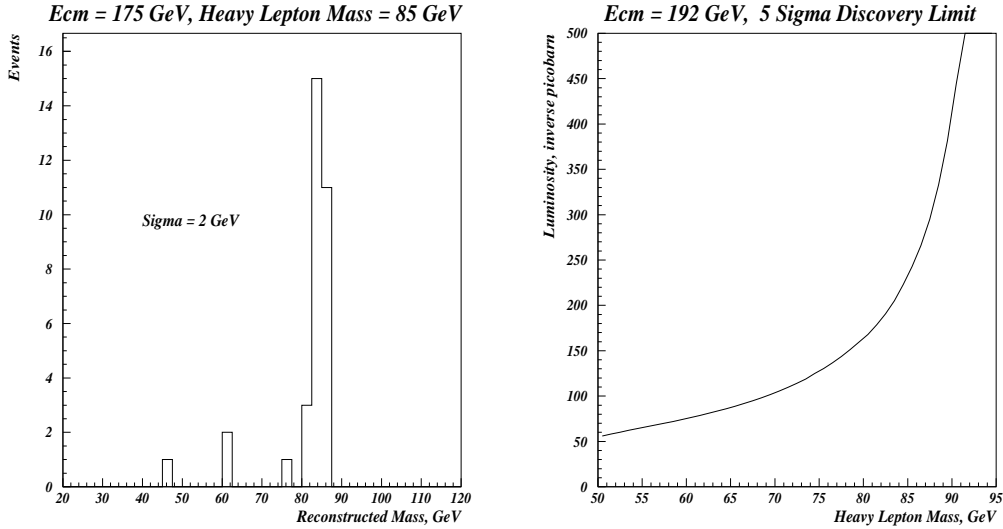
Figure 22: *Left panel: mass reconstruction for $N\overline{N}$ for the process of eq. 2.2. Right panel: the luminosity needed for heavy neutrino 5σ discovery, as a function of N-mass, for $\sqrt{s} = 192$ GeV. The limits for $\sqrt{s} = 175$ GeV are similar, but the mass reach is less.*

2.2.1 Pair Production

Since the introduction of sequential fermions would still have all flavour changing neutral currents (FCNC) to be vanishing at the tree level[1], at LEP2 such particles may only be pair-produced[2] through s-channel diagram(s) mediated by γ/Z. Keeping in mind the expected improvement in the Tevatron bounds, it is thus not very interesting to look for heavy quarks at LEP2. We may thus safely concentrate on lepton pairs only. Total cross sections are in the range 1–4 pb until quite close to the kinematic limit.

The only tree-level decay mode for a fourth-generation lepton proceeds via the charged current interaction. We then make the assumption that the dominant decay is to one of the SM leptons and not to the heavy isospin partner. If the latter were the case, the partner itself should be sought. It should be noted that even if the mixing angle (ζ) with the light leptons is small, the heavy lepton would still decay within the detector provided $\zeta \gtrsim 10^{-6}$.

While a heavy neutrino can be either a Dirac or Majorana particle, in this note we shall concentrate on the former alternative. For, pair-produced Majorana neutrinos can be easily distinguished by the tell-tale signature of like-sign dileptons with hadronic activity but without

---

[1]While this is not strictly true for the exotics, constraints [69] on FCNC imply that pair production dominates over single production for much of the range $m_f < \sqrt{s}$.

[2]The only exception is the process $e^+e^- \rightarrow N\nu$ for a heavy neutrino N which may proceed through a t-channel W-exchange diagram. We shall discuss this case later.
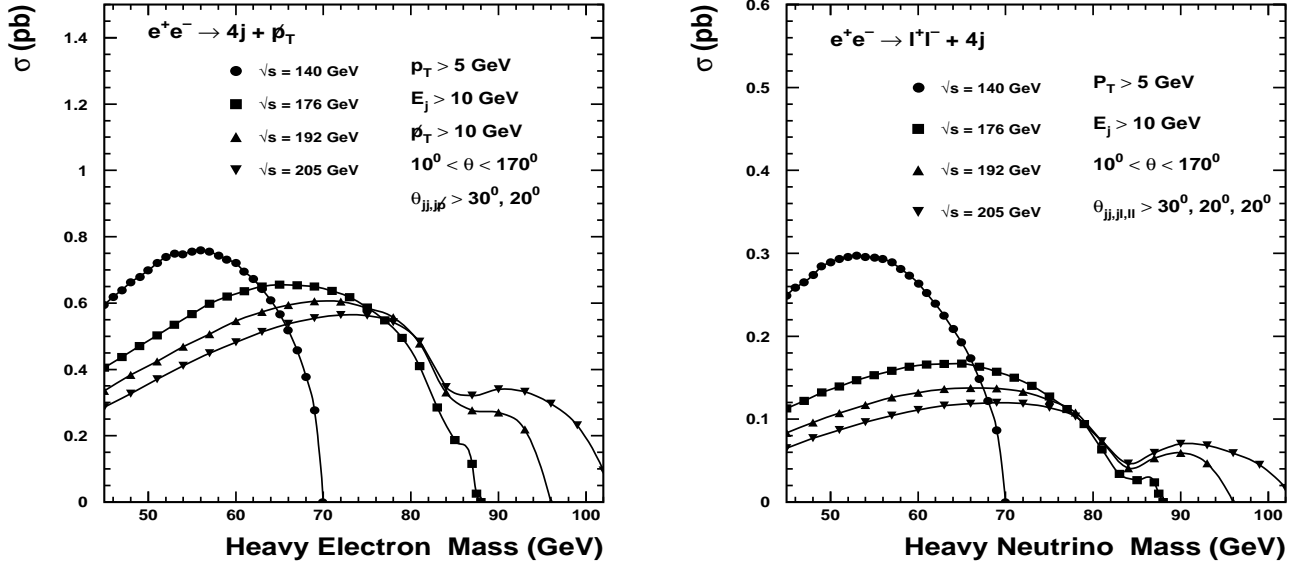
Figure 23: *The effective cross section (at various c.m. energies) for the processes of eqs.2.4 and 2.1, after imposing the cuts of eqs.2.5 and 2.6 respectively.*

any missing momentum. The backgrounds derive from two sources: (*i*) cascade decays of a heavy quark pair (say $b\bar{b} \to ce^-\bar{\nu}\bar{c}q_i\bar{q}_j \to e^-e^-\nu\nu +$ jets) or (*ii*) effects like $B\text{-}\overline{B}$ mixing. They could be eliminated by a combination of isolation cuts and imposition of an upper bound on missing momentum. For a pair of heavy Dirac neutrinos the possible signals are

$$e^+e^- \quad \to \quad N\overline{N} \to l_i^+ l_i^- W^{(*)} W^{(*)} \to l_i^+ l_i^- + 4\,\text{jets} \tag{2.1}$$

$$e^+e^- \quad \to \quad N\overline{N} \to l_i^+ l_i^- W^{(*)} W^{(*)} \to l_i^+ l_i^- l_a + 2\,\text{jets} + \not{p}_T \tag{2.2}$$

$$e^+e^- \quad \to \quad N\overline{N} \to l_i^+ l_i^- W^{(*)} W^{(*)} \to l_i^+ l_i^- l_a^- l_b^+ + \not{p} \tag{2.3}$$

where $\not{p}_T$ denotes missing transverse momentum and the generation index i is determined by the dominant mixing. In this study we concentrate on $l_i = e/\mu$ as the efficiency for τ–detection is low. The purely leptonic channel contains two neutrinos, so mass reconstruction is not possible. Both the other channels have been studied, and a typical mass reconstruction [72] is shown in fig. 22. Derived from the $3l + 2j$ channel, the events are selected by requiring enough hadronic activity to form two jets plus three isolated leptons (< 5 GeV hadronic energy within a cone of $30°$ around the track) above 3 GeV. The lepton (one of the two like-sign ones) associated to the hadronically decaying W is identified by requiring it to have $E_l \sim E_{beam} - E_{had}$. The hadronic energy is then improved by fitting to this relation, and the neutrino identified with the improved $\not{p}$. Background from ZZ is further reduced by rejecting events in which the same-flavour lepton-pair invariant mass is within 5 GeV of the Z-mass. Backgrounds from all SM processes are estimated as 4.8 ± 2.0 events for 500 pb^{-1} and signal efficiencies are around 25% (inclusive of branching ratio, cut efficiency and geometrical acceptance) over a wide range of N-masses. The expected 5σ discovery limits at 192 GeV are shown in fig. 22. While the cross sections are larger for $E\bar{E}$ production, detection is more difficult. Since the distinctive
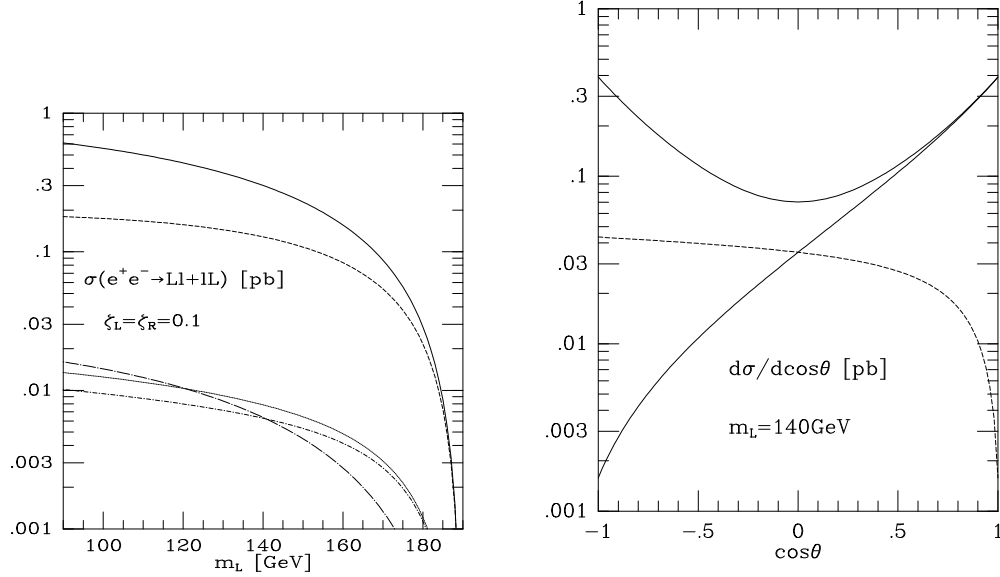
Figure 24: *Total cross section (a) and angular distribution (b) for the single production of exotic leptons in association with their ordinary light partners at LEP2 with $\sqrt{s} = 190$ GeV. The solid (dashed) lines are for first generation neutral leptons with a left–handed (right-handed) mixing, the long-dashed-dotted line is for second/third generation leptons with a left–handed or right-handed mixing, and the dotted (dot-dashed) lines are for first generation charged leptons with a left–handed (right-handed) mixing. For the angular distribution the symmetric solid curve is for a Majorana neutrino.*

signature is

$$e^+e^- \to E\overline{E} \to \nu_i\bar{\nu}_i W^{(*)}W^{(*)} \to 4\,\text{jets} + \not{p}_T, \qquad (2.4)$$

direct mass reconstruction is impossible and a detailed fitting procedure would be needed to determine the mass. In fig. 23 we show the effective cross section [73], after the cuts

$$p_T(j) > 5\text{GeV}, \quad E(j) > 10\text{GeV}, \quad \not{p}_T > 10\text{GeV}, \quad 10° < \theta_j < 170°, \quad \theta_{jj} > 30°, \quad \theta_{j\not{p}} > 20°. \qquad (2.5)$$

With these cuts the SM background (estimated with MadGraph and verified with GRACE) falls to well below 1 fb. With an integrated luminosity of 300pb^{-1}, it should be possible to probe up to $m_E \approx \sqrt{s}/2$. With similar cuts,

$$p_T(j,l) > 5\text{GeV}, \quad E(j) > 10\text{GeV}, \quad 10° < \theta_j, \theta_l < 170°, \quad \theta_{jj} > 30°, \quad \theta_{ll}, \theta_{lj} > 20°, \qquad (2.6)$$

the $N\overline{N}$ channel yields the effective cross section also shown in fig. 23.

2.2.2 Single Production

Introduction of exotic fermions, on the other hand, opens up the possibility of tree-level FC-NCs. This has the immediate consequence of allowing single production of a heavy fermion in association with a SM particle. While most such productions proceed through a s-channel Z^0-mediated diagram, for heavy leptons that have a direct coupling with the electron, there is the additional contribution from t-channel diagrams (W-mediated for $N\nu$ production and Z^0-mediated for eE). For such leptons (to be called "first generation exotics" henceforth), the production cross section can be significantly higher. In fig. 24, we exhibit the mass-dependence of the cross section for various choices of exotic leptons [74]. To be concrete, the left- (right-) handed mixing parameters are assumed to have the most optimistic value of $\zeta_{L,R} = 0.1$. As we see from the figure, the cross sections for the "second and third generation" exotics are below observable levels. As can be expected, the cross sections for quark-production (Qq) are of similar magnitude. We thus reach the conclusion that irrespective of the quantum numbers and the production mode, LEP2 is unsuitable for exploring possible heavy quarks.

While it is obvious that the El production cross section is very small and with LEP2 luminosities we can hope to gain over pair production only by a few GeVs, the signals, nonetheless, are interesting. The heavy lepton E may now have both charged current (final state $l\nu + 2$ jets) and neutral current (final state $l^+l^- + 2$ jets) decays. The latter channel is better suited for mass reconstruction. The main backgrounds arise from $l\nu W$ and $l^+l^- Z$ production respectively. While these may be eliminated by simple cuts, the signal itself is reduced to uninteresting levels.

Returning to the first generation case, we may be more optimistic. Again N can decay both through charged current (final state $l\nu + 2$ jets) and neutral current (final state $\nu\bar{\nu} + 2$ jets) channels, the former being more suitable for mass reconstruction. Events are selected by requiring an isolated identified charged lepton and missing momentum. Then the hadronic activity (jets) is required to be consistent with an on-shell W, while the invariant mass of the electron and $\not{p}$ is inconsistent with an on-shell W. The corresponding SM background (mostly W^+W^-) is reduced to a very low level. The heavy neutrino mass is found from the invariant mass of all the visible particles, see fig. 25(left), obtained from a full simulation in the OPAL detector Monte Carlo [75]. Limits derived from a full simulation in the ALEPH detector Monte Carlo, using a similar analysis, are shown in fig 25(right).

2.3 Excited Leptons

As the spectrum of the excited fermions (F^*) depends crucially on the dynamics of the particular theory in question, the lowest lying excited states can have various spin and isospin quantum numbers. In this study we shall restrict ourselves to spin 1/2 and isospin 0 or 1/2 (other cases have been discussed in ref. [74]). If we assume that the excited states acquire mass above the EW breaking scale (so as to motivate the rather large mass gap), they necessarily would have vector-like couplings [76]. The alternative is to assume a chirality structure identical to the ground state fermions. This is a more conservative choice from the experimentalist's point of
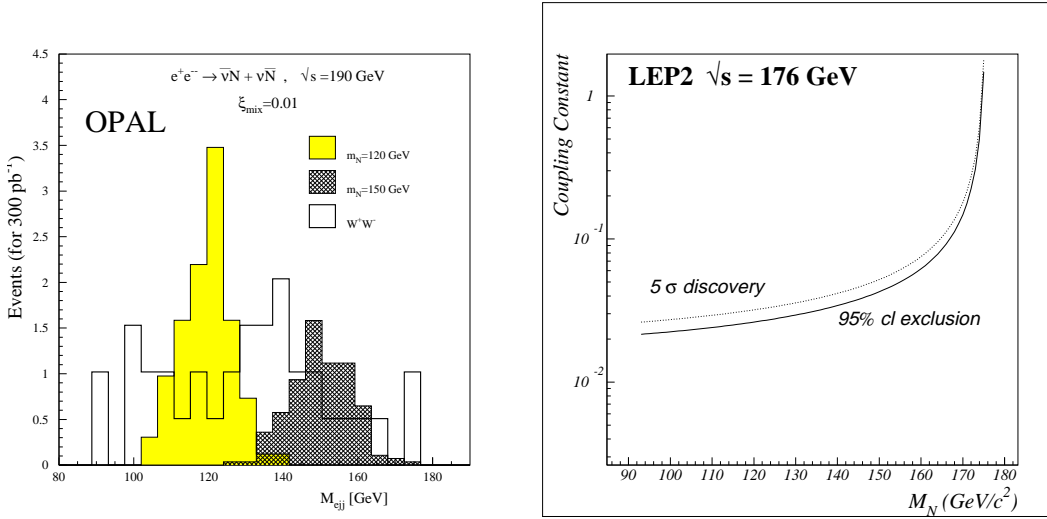
Figure 25: *The singly produced first generation heavy neutrino: reconstructed invariant masses (left) with W^+W^- background at 190 GeV, and (right) limits for 176 GeV*

view as it leads to lower production cross sections. We shall examine both cases in some detail.

Apart from the gauge couplings (governed by the quantum numbers), these particles would also couple to the ground states. As the relevant piece of the interaction Lagrangian has the structure of a magnetic form factor, (and hence is of dimension 5), its strength is determined by f_i/Λ, where Λ is the compositeness scale and f_i are dimensionless coupling constants that may differ for the different gauge bosons. The presence of such couplings allow the excited fermions to decay to their ground state partners and a photon (or gluon in case of quarks).

2.3.1 Pair Production

The pair production cross sections are dominated by s-channel diagrams involving γ and Z exchange. While e^* or ν_e^* production can receive contributions from the magnetic piece of the Lagrangian, for the allowed range of f_i [6], these terms are non-negligible only for $\sqrt{s} \sim \Lambda$. The production rates are thus similar to those for the heavy fermions. The presence of the radiative decay modes thus provides us with tell-tale signatures, especially in the context of LEP2. The SM background may be further reduced by imposing isolation cuts on the photons. We examine below the specific case of $\ell^* \overline{\ell^*}$ production.

Events with two photons above 10 GeV and either two or four tracks are required, all isolated from each other by a cone of at least 25°, with the exception of the track triplet, that must be a τ candidate. Signal events were simulated by smearing Monte Carlo 4-vectors in accordance with the ALEPH detector resolution for tracks and photons, after appropriate 'losses', such as photon conversion. Background events were looked for, using standard EW
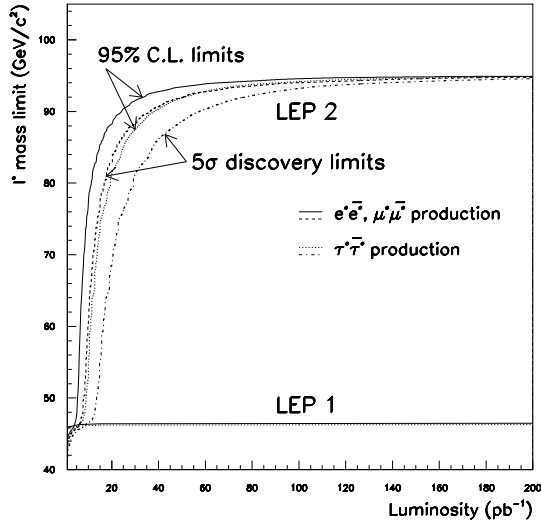
Figure 26: *Limits for excited lepton pairs, decaying radiatively at LEP2 (190 GeV): 205 GeV is very similar, with more mass reach.*

generators, and none were found, but the generators are not fully adequate to estimate the rate, and the program of ref. [77] was used to confirm this prediction. Because of the predominance of γ/Z at masses below the nominal centre of mass energy, it is essential to use events in which the visible energy is deficient; however, with energy- and momentum-conserving reconstruction techniques [78], the energy, E_0, of the most energetic photon below the polar angular acceptance threshold can be estimated, and used in reconstructing the event.

Additionally, when events with two energetic photons and two leptons are found, it is required that there is one way of combining lepton and photon candidates such that the invariant masses of the two lepton-photon pairs have a difference which is smaller than 2σ of the resolution (improved by rescaling events, using energy- and momentum-conservation) as the ℓ^*s produced should be identical. There is significant background prior to this last cut, but after it the background is very small, and the signal efficiency remains high: 67% for $e^*\overline{e^*}$ and $\mu^*\overline{\mu^*}$, and 50% for $\tau^*\overline{\tau^*}$, which has poorer resolution. Limits for exclusion and discovery at $\sqrt{s} = 190$ are shown in fig. 26.

2.3.2 Single Production

Occurring on account of the f_i terms, these channels would allow us to probe for F^* masses close to the c.m. energy. In fig. 27, we show the total cross sections for different choices of vector-like excited leptons at a c.m. energy of 190 GeV. The largest production rate occurs for
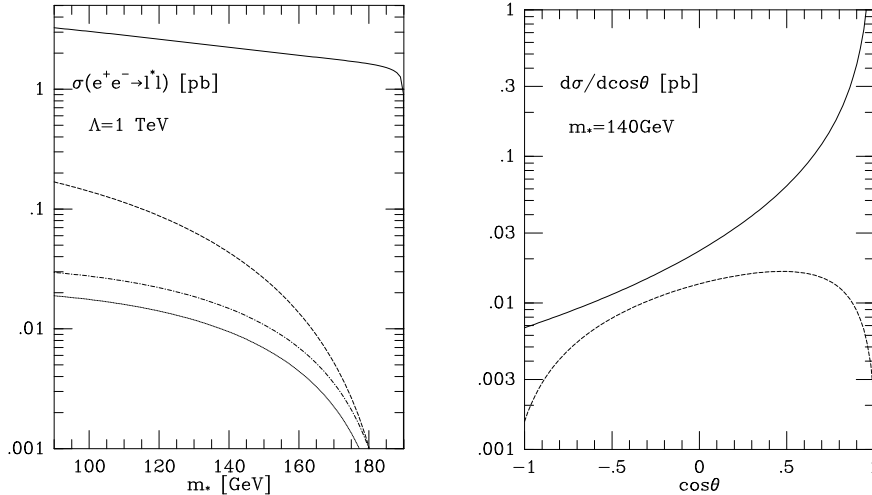
41

Figure 27: *Total cross section (a) and angular distribution (b) for the single produc-
tion of vector-like excited leptons in association with their ordinary light partners at
LEP2 with $\sqrt{s} = 190$ GeV and $\Lambda = 1$ TeV. The solid (dashed) lines are for first gen-
eration charged (neutral) excited leptons and the dotted (dash–dotted) lines are for the
second/third generation charged (neutral) excited leptons.*

the e^* due to the t-channel photon exchange. Compared to the other charged leptons this has
a two-order of magnitude enhancement. An analogous statement may be made about ν_e^* (as a
consequence of the W exchange contribution) when compared to the other excited neutrinos.
Similar statements also hold for the chiral F^*, and, henceforth, we shall concentrate on this
possibility.

Charged excited leptons[3] should be looked for by exploiting their electromagnetic decays
leading to a signal

$$e^+ e^- \to l l^* \to l^+ l^- \gamma \tag{2.7}$$

All signal and background (EW) events were fully simulated in the ALEPH detector Monte
Carlo. To qualify, an event had to be comprised of a dilepton pair in addition to one and
only one photon above 10 GeV. Isolation criteria were held to be the same as in the previous
section, and a possible low angle photon was reconstructed. Examples of the results are shown
in fig. 28. It must be borne in mind that the couplings f_γ/Λ and f_Z/Λ are *a priori* different.
To eliminate one variable, the relationship used in ref. [66] was assumed. The lower sensitivity
for the $\tau^* \tau$ case is due to the greater difficulty in reconstructing the events.

For the particular case of e*e production, the photon and Z contribution can be unrav-

---

[3]For excited neutrinos, the situation is similar to that of exotic neutrinos (although the angular distributions
are different, as shown in fig. 27) and one has to look for $e\nu jj$ events. A detailed analysis has not been performed
here. Note that the single photon signal has a large associated background.
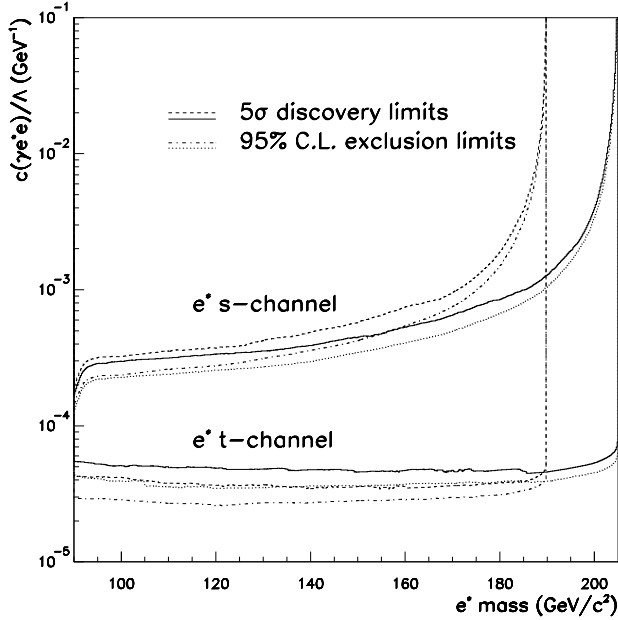
Figure 28: *Exclusion and discovery limits (at 190 and 205 GeV) in the mass-coupling plane for singly produced chiral* e*. *The two sets derive from 2–track ("s–channel) and 1–track ("t–channel) signals respectively.* $\mu^*\mu$ *limits are almost identical to* e*e *(2–track), and* $\tau^*\tau$ *only a little worse.*

eled by exploiting the difference in their angular distributions. Since the t-channel γ–exchange diagram, unlike the others, gives a very forward peaked contribution, it dominates the configurations wherein one electron essentially disappears down the beam pipe. The final state is thus of the form $(e^+)e^-\gamma$ and the main background is from higher order processes in QED and misidentifications. Following the analysis of ref. [78], the plane defined by the track and the photon is required to be nearly normal to the beam axis and the polar angle corresponding to the missing momentum is required to be less than 2°. Possibility exists though that the missed electron had a polar angle of greater than 2° but was too slow to get into the main tracking detector. This is taken care of by vetoing events with a large excess of hits in the inner tracker (since this corresponds to a "spiralling" electron). The exclusion limit after the imposition of these cuts is shown in fig. 28. As was indicated earlier, this particular configuration is much more sensitive to the presence of e* than those where both the electrons are visible in the main detector.

2.3.3 Virtual Effects

While the single production channels raise the mass reach of the machine to nearly the kinematical limit, it is interesting to ask the question if one could explore masses beyond the c.m. energy, albeit at the cost of accommodating a somewhat larger coupling constant. The only existing constraints for $m_{e^*} > 130$ GeV are derived from one-loop corrections to low-energy observables such as $g-2$ of the electron (see references quoted in [6]) and are subject to theoretical uncertainties. AT LEP2, a particular window is provided by the possible t-channel exchange of a virtual e*. The signal consists of a distribution of 2-photon final states that has an excess at high polar angle (on account of the large mass of the e*), when compared to the EW expectation. In practice, 3-photon final states (first order initial state radiative correction) have to be taken into account as well, and the analysis uses the two most energetic photons and the angle between them in their centre of mass frame, θ^*. To perform a quantitative analysis, we adopt the the maximum likelihood method [6]. The cross section is parametrized [79] in terms of the e^* mass and a dimensionless effective coupling λ and the resultant expression compared to the actual (simulated) data. Assuming an integrated luminosity of 500 pb^{-1}, we find that for $\lambda = 1$ one can achieve 95% C.L. mass exclusion limits of $\sim 250(300)$ GeV at $\sqrt{s} = 190(205)$GeV.

3 Leptoquarks

Leptoquarks carry, simultaneously, lepton and quark quantum numbers. They naturally appear in unified and composite models [80] and mediate lepton–quark transitions. For this study we adopt the phenomenological framework suggested in ref. [81] which involves a minimal number of model assumptions. It is designed for spin 0 and 1 leptoquarks with the most general dimensionless couplings to lepton-quark pairs which are $SU(3)_c \times SU(2)_L \times U(1)$ symmetric, family–diagonal, and baryon and lepton number conserving. The corresponding couplings to the EW gauge bosons are given in ref. [82]. One can distinguish two classes of leptoquarks: color–triplets with fermion number 2 decaying into lepton–quark final states and color–antitriplets with fermion number 0 decaying into lepton–antiquark final states. The weak isospin varies from 0 to 1. A complete list of the possible species and their quantum numbers can be found in refs. [81, 82].

Experimentally, the existence of leptoquarks is constrained indirectly by low-energy data [83] and precision measurements of the Z widths [84], and by direct searches at high energies [85, 86, 87, 88]. In particular, rare processes and processes which are forbidden in the Standard Model provide stringent bounds on $\frac{\lambda}{m_{LQ}}$, where λ denotes the leptoquark–fermion Yukawa couplings. Essentially, below the TeV mass range and for λ of the order of the electromagnetic coupling, the only allowed leptoquarks are those which couple only to a single fermion generation and, for the two lighter generations, either only to the left- or to the right-handed components. HERA experiments exclude first generation scalar leptoquarks up to $m_{LQ} = 250$ GeV for $\lambda = e$ $(\alpha = \frac{e^2}{4\pi})$ [85]. Bounds which are independent of λ and therefore unescapable come from

LEP and TEVATRON. The LEP experiments set a mass limit of 45.6 GeV for any leptoquark species [86]. Searches with the D0 detector exclude first generation scalar leptoquarks below $m_{LQ} = 133$ GeV [87], while the CDF experiment puts a bound on second generation scalar leptoquarks at $m_{LQ} = 131$ GeV provided these leptoquarks decay to electron (muon) plus jet with 100% branching ratio [88]. Since there is at least one state in each isospin multiplet with $Br(LQ \to l + jet) \geq 0.5$ where $l = e$ or μ, the absolute lower mass limit for first (second) generation scalar leptoquarks is 120 GeV (96 GeV), at least if the members of a multiplet are nearly mass–degenerate. Otherwise, states decaying exclusively into $\nu+$ jet final states are only required to respect the less severe LEP1 mass limit. For sufficiently small λ, the LEP1 bound is also the only one applying to third generation leptoquarks.

At LEP2, leptoquarks can be pair–produced via s–channel γ and Z exchange and, in the case of first generation leptoquarks carrying the electron number, also via t–channel exchange of a u or d–quark. The latter process involves the unknown Yukawa coupling λ. The production cross section depends very much on the leptoquark quantum numbers [82]. At $\sqrt{s} = 190$ GeV and for $m_{LQ} = 80$ GeV it varies from 0.04 pb for the scalar isosinglet S_1 with charge $-\frac{1}{3}$ to 12 pb for the vector isotriplet U_3 with charge $+\frac{5}{3}$ (possible t–channel contributions are disregarded). Here, we follow the notation introduced in [81]. Furthermore, leptoquarks in the LEP2 mass range are very narrow. The partial width for a massless decay channel is expected to be of the order of 100 MeV for $\lambda = e$.

The signatures for leptoquark pair–production and decay are: *i)* two electrons (muons) plus two hadronic jets; *ii)* one electron(muon), two hadronic jets, and missing energy; *iii)* two hadronic jets and missing energy; *iv)* two tau leptons plus two hadronic jets. Given the Tevatron bounds pointed out above, the focus is on the last two signals. To estimate the acceptance for leptoquark final states we have written a Monte Carlo program and generated events for $m_{LQ} = 50 - 80$ GeV, $0 < \lambda_{L,R}/e < 1$, and $\sqrt{s} = 150$, 175 and 190 GeV. The generator is based on the analytical formulae for cross sections and angular distributions given in ref. [82]. Initial state radiation is included. Fragmentation is implemented according to JETSET 7.3 [28].

The following background processes have been considered and generated for $\sqrt{s} = 150$, 175 and 190 GeV using Pythia 5.7 [28]: $e^+e^- \to W^+W^-, We\nu, ZZ, Zee$, and two-photon processes. The numbers of generated events correspond to an integrated luminosity of 500 pb^{-1}, except for the two-photon processes, where they correspond to only 20 pb^{-1}. The events were passed through the standard L3 simulation and reconstruction program [89].

Two electrons (muons) and two jets

The signal events are required to consist of two energetic electrons (muons) with energies greater than 20 GeV, and two hadronic jets. Furthermore, we require the total visible energy to be greater than $0.9 \times \sqrt{s}$. The ZZ background is suppressed by demanding that the invariant mass of the two leptons is outside the Z mass window. Since this cut is not efficient if one Z bosons is produced off-shell, we require in addition that the difference between the two reconstructed leptoquark mass values is less than 4 GeV. The masses are determined using

energy–momentum conservation. We find that the mass of an 80 GeV leptoquark of the first generation can be reconstructed with a resolution of about 0.5 GeV.

One electron (muon) and two jets

In this channel, we require the events to consist of one energetic electron (muon) with energy greater than 20 GeV, and two hadronic jets. Furthermore, we request the total visible energy to be greater than $0.5 \times \sqrt{s}$ and less than $0.9 \times \sqrt{s}$. The WW and $We\nu$ backgrounds are suppressed by demanding that the invariant masses of the two jets and of the lepton-neutrino pair is outside the W mass window, and that the difference between the two reconstructed leptoquark mass values is less than 8 GeV. In order to calculate the leptoquark masses, we determine the missing momentum from energy–momentum conservation. The leptoquark mass resolution turns out to be about 2 GeV.

Two neutrinos and two jets

This is a particularly important channel. The signal events are selected by requiring that the event consists of two hadronic jets with a total energy less than $0.8 \times \sqrt{s}$ and that it contains no electrons with energy greater than 20 GeV. Furthermore, the event multiplicity has to be greater than four, and the polar angle of the missing momentum has to be larger than 30° or less than 150°. The background in this channel is composed of ZZ events with one Z boson decaying into two neutrinos, WW and $We\nu$ events with one W boson decaying hadronically, and two-photon events. To remove the two-photon events, we require the total energy in the event to be greater than $0.4 \times \sqrt{s}$, and the minimal jet energy to be greater than 10 GeV. The background from events in which some particles are not correctly reconstructed in the detector is removed by demanding the calorimetric energy in a 30° cone around the missing momentum to be less than 1 GeV. No charged track must be found in this cone. We find about ten ZZ, WW and $We\nu$ events which survive the above cuts. These can be removed by a cut on the invariant jet–jet mass, $M_{jj} \frac{\sqrt{s}}{E_{vis}} < min(\sqrt{s} - m_Z, \; m_W) - 10$ GeV.

Two tau leptons and two jets

This signal is the most difficult one to recover from the WW, ZZ, and $We\nu$ background. We require that the event consists of four jets, with a minimal jet energy greater than 8 GeV and two jets having multiplicity one. Furthermore, the total energy in the event must be greater than $0.5 \times \sqrt{s}$ and less than $0.9 \times \sqrt{s}$. Finally, we look for the most isolated track with momentum greater than 3 GeV, and require that there is no other track inside a 20° cone around this track. The calorimetric energy inside that cone has to be more than 5 GeV, and the difference of the calorimetric energies in the 30° and 20° cones around the track has to be less than 1 GeV.

Table 4 shows the estimated acceptance and number of surviving background events for different leptoquark decay channels. Using these numbers and the leptoquark production cross sections, we estimated the 5σ discovery limits as a function of the integrated luminosity. Some illustrative results are shown in fig. 29. Note that the large variation of the discovery limit for the first generation leptoquark S_1^e is mainly due to the variation of the Yukawa coupling λ.

46

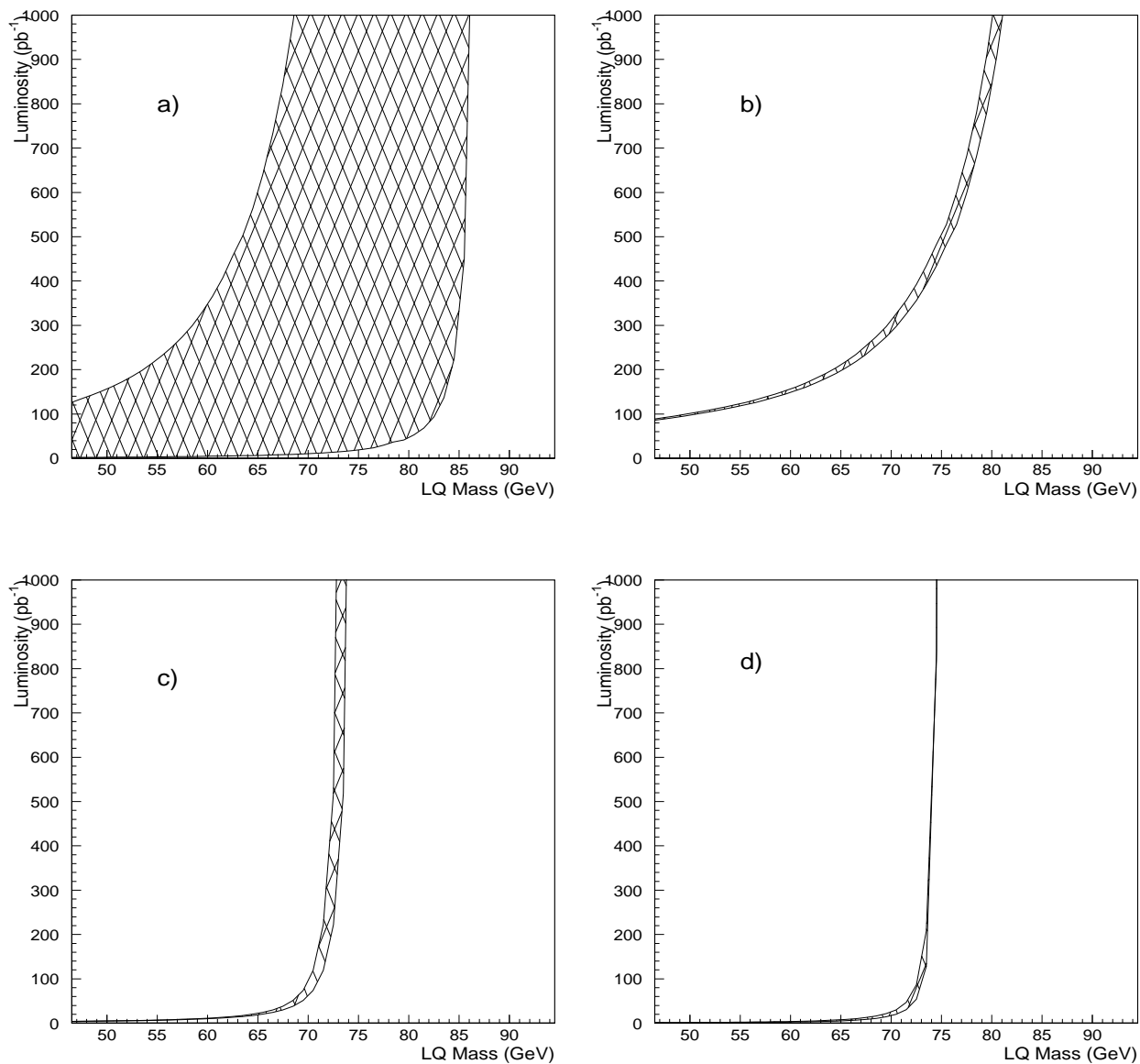Figure 29: 5σ discovery limits for a) S_1^e at 175 GeV, b) S_1^τ at 190 GeV taking $Br(S_1^\tau \to \nu_\tau b) = 1$, c) S_3^τ (4/3) at 150 GeV, and d) U_1^μ at 150 GeV. The shaded areas show the effect of varying the Yukawa couplings $\lambda_{R,L}/e$ from zero to unity, and the acceptance within the estimated range given in table 4.

Decay Channel	Acceptance (%) for $50 < M_{LQ} < 80$ GeV	Background at 150-190 GeV
$e^+e^-q\bar{q}$	39 to 45	0-1 ZZ
$e\nu q\bar{q}$	22 to 25	3-5 WW
$\mu^+\mu^-q\bar{q}$	42 to 48	0
$\mu\nu q\bar{q}$	22 to 25	4-6 WW
$\nu\bar{\nu}q\bar{q}$	20 to 23	1 2γ, 1-3 $ZZ,WW,We\nu$
$\tau^+\tau^-q\bar{q}$	11 to 12	10-13 WW,ZZ

Table 4: *Acceptance and number of background events for different leptoquark signals assuming an integrated luminosity of 500 pb^{-1}.*

To summarize, a feasibility study on the search for leptoquarks at LEP2 with the L3 detector has been carried out. We have considered different leptoquark species and signatures. The main result is that after applying the appropriate cuts all signals except the one in the $\tau\tau$ plus two-jet channel are practically background–free. In the latter case, we expect 10 to 20 background events for 500 pb^{-1}. Since the existing mass limits for leptoquarks decaying into electron (muon) plus jet are already beyond the LEP2 energy range, the leptoquark species relevant for LEP2 searches are those which decay into τ plus jet and ν plus jet.

4 The BESS Model for Dynamical EW Symmetry Breaking

It is a common theoretical idea that the parameterization of the mechanism of EW mass generation in terms of scalar couplings may be the effective low-energy manifestation of more fundamental dynamics. The new dynamics may, for instance, have the form of a new strong interaction [90], [91]. The idea which leads to the formulation of the BESS model (Breaking Electroweak Symmetry Strongly) [92] assumes the existence of a strongly interacting longitudinal-scalar sector, and enables one to parametrize the most relevant phenomenological effects, without assuming an explicit dynamical realization.

We discuss the sensitivity of LEP2 to possible new physics from a strong EW symmetry breaking sector. The model proposed in ref. [92] is an effective lagrangian description of Goldstone bosons and new vector resonances as the expectedly most visible manifestations at low energy of the strongly interacting sector. In particular we will focus on the case in which the new resonances are degenerate in mass (neglecting the weak corrections) [93]. This degenerate model has the interesting feature of allowing for a strong EW resonant sector at relatively low energies, while satisfying the severe constraints from existing LEP, SLC and CDF
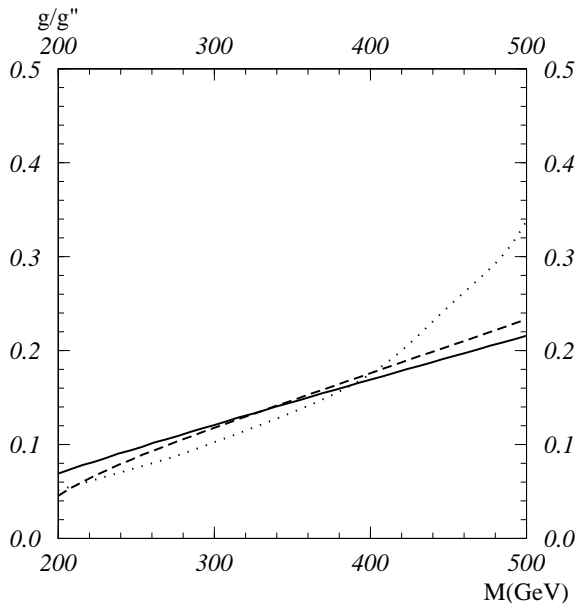
Figure 30: *95% C.L. upper bounds on g/g'' vs. M from LEP1 data (continuous line) and CDF data (dotted line) compared with the expected bounds from LEP2 (dashed line).*

data. This type of realization corresponds to a maximal symmetry $[SU(2) \otimes SU(2)]^3$. After gauging the standard $SU(2) \otimes U(1)$, the model describes the ordinary standard gauge bosons $W^\pm$, Z and γ and, in addition, two new triplets of massive gauge bosons, $L^\pm$, L_3, $R^\pm$, R_3, self-interacting with gauge coupling constant g''. These heavy resonances, as a consequence of the chiral symmetry, are degenerate in mass M in the $g'' \to \infty$ limit. The main property of the degenerate BESS lagrangian is that it becomes identical to that of the Standard Model (taken in the formal limit of infinite Higgs mass) for $M \to \infty$. Therefore, differently from ordinary BESS, the heavy mass decoupling occurs. Concerning the couplings to fermions, we do not introduce extra parameters. In this way the new bosons are coupled to fermions only through the mixings with the ordinary gauge bosons. The peculiar feature of degenerate BESS is that for any M the new bosons are not coupled to the Goldstone bosons which are absorbed to give mass to $W^\pm$ and Z. As a consequence, the channels $W_L Z_L$ and $W_L W_L$ are not strongly enhanced as it usually happens in models with a strongly interacting symmetry breaking sector and this implies larger branching ratios of the new resonances into fermion pairs. Degenerate BESS would thus be much more evident experimentally than ordinary BESS, at the appropriate energy, but at the same time much less constrained by existing EW limits.

Let us now discuss how new resonance effects modify the observables which are relevant for the physics at LEP and Tevatron. For LEP physics the modifications due to heavy particles are contained in the so-called oblique corrections. In the low-energy limit, one can expand the vacuum polarization amplitudes in q^2/M^2 where M is the heavy mass, and they can be

49

parametrized, for example, in terms of the ϵ parameters [12, 15]. At the leading order in q^2/M^2 the new contribution of the model to all these parameters is equal to zero. This is due to the fact that in the $M \to \infty$ limit, the new states decouple [93]. We can perform the low-energy limit at the next-to-leading order and study the virtual effects of the heavy particles. Working at the first order in $1/g''^2$ we get $\epsilon_1 = -(c_\theta^4 + s_\theta^4)/(c_\theta^2)\,X$, $\epsilon_2 = -c_\theta^2\,X$, $\epsilon_3 = -X$ with $X = 2(m_Z{}^2/M^2)(g/g'')^2$. All these deviations are of order X and therefore contain a suppression both from $m_Z{}^2/M^2$ and $(g/g'')^2$. The sum of the SM contributions, functions of the top and Higgs masses, and of these deviations has to be compared with the experimental values for the ϵ parameters, determined from the all available LEP data and the m_W measurement at Tevatron [94]: $\epsilon_1 = (3.8 \pm 1.5) \cdot 10^{-3}$, $\epsilon_2 = (-6.4 \pm 4.2) \cdot 10^{-3}$, $\epsilon_3 = (4.6 \pm 1.5) \cdot 10^{-3}$. Taking into account the SM values $(\epsilon_1)_{SM} = 4.4 \cdot 10^{-3}$, $(\epsilon_2)_{SM} = -7.1 \cdot 10^{-3}$, $(\epsilon_3)_{SM} = 6.5 \cdot 10^{-3}$ for $m_t = 180\ GeV$ and $m_H = 1000\ GeV$, we find, from the combinations of the previous experimental results, the 95% CL limit on g/g'' versus the mass M given by the solid line in fig. 30. The excluded region is above the curve. We see that there is room for relatively light resonances beyond the usual SM spectrum. The same analysis done for the ordinary BESS model gives bounds which are much more stringent ($g/g'' < 0.03$ for any value of M). In fig. 30 the limits on the degenerate model parameter space derived from CDF data are also shown (dotted line). The curve was obtained using the CDF 95% C.L. limit on the W' cross section times the branching ratio and comparing this limit with the predictions of our model. The limit from CDF is more restrictive for low resonance masses with respect to the LEP limit.

Concerning the bounds which would come from LEP2 assuming no deviations from the SM within the estimated errors, we have analyzed cross sections and asymmetries for the channel $e^+e^- \to f^+f^-$ in the SM and in degenerate BESS at tree level. We have first considered the following observables: total hadronic and muonic cross sections σ^h, σ^μ; the forward-backward asymmetries $A_{FB}^{e^+e^- \to \mu^+\mu^-}$, $A_{FB}^{e^+e^- \to b\bar{b}}$; m_W measurement. In fig. 30 we show LEP2 limits obtained considering $\sqrt{s} = 175$ GeV and an integrated luminosity of $500pb^{-1}$, combining the deviations coming from the previous observables (dashed line). For m_W we assume a total error (statistical and systematic) $\Delta m_W = 50$ MeV. For σ^h the total error assumed is 2%. For all the other observable quantities we assume only statistical errors. The comparison with the bounds from LEP and CDF shows that LEP2 will not improve the existing limits on degenerate BESS (the same conclusions hold for the ordinary BESS model). We have also considered the possibility of having polarized beams at LEP2 by analyzing the left-right asymmetries: $A_{LR}^{e^+e^- \to \mu^+\mu^-}$, $A_{LR}^{e^+e^- \to b\bar{b}}$, $A_{LR}^{e^+e^- \to had}$. However the improvement with respect to the unpolarized case is only marginal. Moreover considering the option of LEP2 at $\sqrt{s} = 190$ GeV does not modify the result in a significant way.

5   Virtual Effects

This section is devoted to the study of virtual effects from new physics in the cross section for $e^+e^- \to W^+W^-$. We have focused on two simple SM extensions: i) the SM plus an ex-

tra doublet of heavy quarks, exact replica of the SM counterparts as far as their EW and strong quantum numbers are concerned; *ii*) the MSSM with relatively heavy (above the production threshold) EW gauginos and higgsinos, and very heavy (decoupled) squarks, sleptons and additional higgses. In both models the 1-loop corrections to the process in question are concentrated in vector-boson self-energies and three-point functions, which makes it possible to analyze the interplay between the two contributions. Box corrections are obviously absent in the first model, while they are negligibly small in the second case, provided that the scalar masses are sufficiently large. Then the only relevant contributions remain those of gauginos and higgsinos to vertices and self-energies.
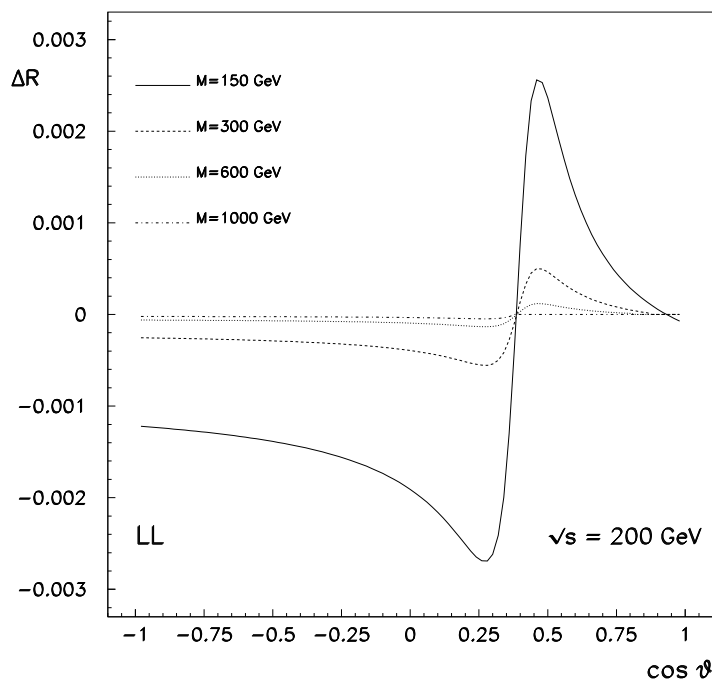

Figure 31: *Relative deviations in the differential cross section, due to gauginos contribution (LL channel) for* M_2 = 150, 300, 600, 1000 GeV

To avoid conflicts with the LEP1 constraints on the ϵ parameters [12, 15], we consider the new doublet in *i*) as mass degenerate [95]. Model *ii*) respects LEP1 bounds for arbitrary masses of the new particles, except for the case when they are very light and close to the production threshold of LEP1 [96]. However for practical purposes we have considered the case of degenerate EW gauginos of mass M_2 and degenerate higgsinos of mass μ, in which the mixing terms among gauginos and higgsinos are negligible $(M_2, \mu >> m_W)$.

After the inclusion of the 1-loop corrections due to the new particles and of the appropriate counterterms, the reduced amplitude for the process at hand is (following the conventions of

ref.[97]):

$\bullet \Delta\lambda = \pm 2$

$$\tilde{\mathcal{M}} \;=\; -\frac{\sqrt{2}}{\sin^2\bar\theta}\delta_{\Delta\sigma,-1}\left[1 - \frac{\sin^2\bar\theta}{\cos 2\bar\theta}\Delta r_W - e_6\right]\frac{1}{1+\beta^2 - 2\beta\cos\Theta} \tag{5.1}$$

$\bullet |\Delta\lambda| \leq 1$

$$\tilde{\mathcal{M}}^\gamma \;=\; -\beta\delta_{|\Delta\sigma|,1}\left[1+\Delta\alpha(s)\right]\left[A^\gamma_{\lambda\bar\lambda} + \delta A^\gamma_{\lambda\bar\lambda}(s)\right]$$

$$\tilde{\mathcal{M}}^Z \;=\; \beta\left[1+\Delta\rho(s) + \frac{\cos 2\bar\theta}{\cos^2\bar\theta}\Delta k(s)\right]\left[\delta_{|\Delta\sigma|,1} - \frac{\delta_{\Delta\sigma,-1}}{2\sin^2\bar\theta(1+\Delta k(s))}\right]\frac{s}{s-m_Z^2}\left[A^Z_{\lambda\bar\lambda} + \delta A^Z_{\lambda\bar\lambda}(s)\right]$$

$$\tilde{\mathcal{M}}^\nu \;=\; \frac{1}{2\sin^2\bar\theta\,\beta}\delta_{\Delta\sigma,-1}\left[1 - \frac{\sin^2\bar\theta}{\cos 2\bar\theta}\Delta r_W - e_6\right]\left[B_{\lambda\bar\lambda} - \frac{1}{1+\beta^2-2\beta\cos\Theta}C_{\lambda\bar\lambda}\right] \tag{5.2}$$

with $\beta = (1-4m_W^2/s)^{1/2}$, Θ is the scattering angle of W^- with respect to e^- in the e^+e^- c.m. frame; σ, $\bar\sigma$, λ, $\bar\lambda$ are the helicities for e^-, e^+, W^- and W^+, respectively; $\Delta\sigma = \sigma - \bar\sigma$; $A^\gamma_{\lambda\bar\lambda}$, $A^Z_{\lambda\bar\lambda}$, $B_{\lambda\bar\lambda}$ and $C_{\lambda\bar\lambda}$ are tree-level SM coefficients listed in table 3 of ref. [97]; $\Delta\alpha(s)$, $\Delta k(s)$, $\Delta\rho(s)$, Δr_W are finite self-energy corrections, appropriate extensions to the center of mass energy $\sqrt{s}$, of the corresponding EW parameters defined in [96, 12, 15] and e_6 is the wave function renormalization of the external W' s lines. Finally, $\delta A^\gamma_{\lambda\bar\lambda}$ and $\delta A^Z_{\lambda\bar\lambda}$ represent the corrections to the trilinear gauge boson vertices. For the models considered, they can be expressed in terms of the CP-invariant form factors $\delta f_i^{\gamma,Z}$ $(i=1,...,4)$ according to the relations:

$$\begin{aligned}
\delta A^V_{++} &= \delta A^V_{--} = \delta f_1^V\\
\delta A^V_{+0} &= \delta A^V_{-0} = \gamma(\delta f_3^V - i\delta f_4^V)\\
\delta A^V_{0-} &= \delta A^V_{0+} = \gamma(\delta f_3^V + i\delta f_4^V)\\
\delta A^V_{00} &= \gamma^2\left[-(1+\beta^2)\delta f_1^V + 4\gamma^2\beta^2\delta f_2^V + 2\delta f_3^V\right]
\end{aligned} \tag{5.3}$$

with $\gamma = \sqrt{s}/2m_W$. Here δf_i^V $(i=1,...,4)$ $(V=\gamma, Z)$ includes both the contribution coming from the 1-loop correction to the vertex VWW and the wave-function renormalization of the external W legs, taken on the mass-shell. This makes the terms δf_i^V finite.

The tree-level SM amplitudes are recovered from the above formulae by taking $\Delta\alpha(s) = \Delta k(s) = \Delta\rho(s) = \Delta r_W = e_6 = \delta A^\gamma_{\lambda\bar\lambda} = \delta A^Z_{\lambda\bar\lambda} = 0$. In the high-energy limit, the individual SM amplitudes from photon, Z and ν exchange are proportional to γ^2 when both the W are longitudinally polarized (LL) and proportional to γ when one W is longitudinal and the other is transverse (TL). The cancellation of the γ^2 and γ terms in the overall amplitude is guaranteed by the tree-level, asymptotic relation: $A^\gamma_{\lambda\bar\lambda} = A^Z_{\lambda\bar\lambda} = B_{\lambda\bar\lambda}$.

When one-loop contributions are included, one has new terms proportional to γ^2 and γ (see $\delta A^\gamma_{\lambda\bar\lambda}$ and $\delta A^Z_{\lambda\bar\lambda}$ in eq. (5.3)) and the cancellation of those terms in the high-energy limit entails relations among oblique and vertex corrections. Omitting, for instance, the gauge boson self-energies such cancellation does not occur any longer and the resulting amplitudes violate the requirement of perturbative unitarity.

On the other hand, one of the possibilities to have appreciable deviations in the cross section is to delay the behaviour required by unitarity. This may happen if in the energy window $m_W << \sqrt{s} \leq 2M$ (M denoting the mass of the new particles) the above cancellation is less efficient and terms proportional to positive powers of γ survive in the total amplitude. Only if γ were sufficiently large, beyond the LEP2 value, could sizeable deviations from the SM be expected.

Figure 31 shows the relative deviation from SM results [98]

$$\Delta R = \frac{\left(\dfrac{d\sigma}{d\cos\Theta}\right) - \left(\dfrac{d\sigma}{d\cos\Theta}\right)_{SM}}{\left(\dfrac{d\sigma}{d\cos\Theta}\right)_{SM}} \tag{5.4}$$

in model ii), relative to the LL channel, as function of $\cos\Theta$ at $\sqrt{s} = 200$ GeV for several values of the gaugino mass M_2 and negligible higgsino contribution ($\mu \gg M_2 \gg m_W$).

The deviations, even in the most favourable case $M_2 = 150$ GeV, are unobservable, being smaller than $3.0 \cdot 10^{-3}$ [99]. Similar magnitudes have been found for the channels TL and TT and when the higgsino contribution is singled out. Only when one considers SUSY particles very close to the production threshold (e.g. $M_2 = 105$ GeV at $\sqrt{s} = 200$ GeV), deviations of the order 1% are obtained. When model i) is considered, the deviations at LEP2 are at the percent level in the LL and TL channels, even smaller in the TT one and in any case well below the observability level.

Finally we would like to mention that at higher energies ($\sqrt{s} = 500$ GeV or even more) the deviations ΔR in model ii) remain at the percent level, making questionable the possibility of observing such effect even in next generation e^+e^- colliders [100]. While more interesting is the case of model i), in which a delay of unitarity in the LL, LT channels, due to γ enhancement factor, gives deviations from SM of the order 10-50 %, for a wide range of new particles masses.

6 CP-odd Correlations at LEP2

Unpolarized (and transversely polarized) e^+e^- collisions can be used for genuine tests of CP invariance at high energies (see, for example [101]). We envisage here statistical tests with observables which change sign under a CP transformation. Measurement of a non-zero mean value of such an observable would signal violation of this symmetry. At LEP2 energies heavy fermion production, $i.e.$ tau pair and $b\bar{b}$ production appear to be interesting channels for such tests (for the case of W^+W^- production, see ref. [102]). It is possible to conceive that non-standard CP-violating interactions induce substantially larger effects for heavy fermions than for light flavours. Moreover, a study of various non-standard models of CP violation shows that models with leptoquark mediated CP violation may induce form factors $d_\tau^{Z,\gamma}$ as large as $10^{-18}ecm$ at LEP2 energies [103].

The first CP symmetry tests at high energies were made by the OPAL and ALEPH collaborations for tau pair production at LEP1. These experiments also obtained an upper bound on the CP-violating weak dipole form factor of the tau lepton [104, 105]. The combined OPAL and ALEPH measurements at the Z resonance yield [106] $|\mathrm{Re}\, d_\tau^Z(\sqrt{s} = m_Z)| < 6.7 \times 10^{-18} ecm$ (95 % C.L.). There is a direct bound on the tau electric dipole moment (EDM), $|\mathrm{Re}\, d_\tau^\gamma(s = 0)| < 4 \times 10^{-16} ecm$ (95 % C.L.), from $\tau\tau\gamma$ events at LEP1 [107]. The most stringent bound on the electric dipole moment (EDM) form factor, $|d_\tau^\gamma(\sqrt{s} = m_Z)| < 5 \times 10^{-17} ecm$ (2σ), has been derived indirectly [108]. However, one can imagine models [101] which invalidate the arguments used for deriving indirect bounds on CP-violating form factors.

Here we wish to point out that, in spite of the limited statistics, one can perform CP tests in tau pair production also at LEP2. These tests are useful because they would provide *direct* information on the weak *and* EDM form factors at about twice the energy of LEP1.

We consider tau pair production with unpolarized e^+e^- collisions at LEP2 energies and their subsequent decays into the following channels:

$$e^+(\mathbf{p}_+) + e^-(\mathbf{p}_-) \to \tau^+(\mathbf{k}_+) + \tau^-(\mathbf{k}_-) \to A(\mathbf{q}_-) + \bar{B}(\mathbf{q}_+) + X, \tag{6.1}$$

where the 3-momenta refer to the overall c.m. frame and $A, B = \ell, \pi, \rho, a_1$ (ρ and a_1 also denote the 2π and 3π states, respectively). CP symmetry tests which are experimentally rather straightforward involve CP-odd observables $\mathcal{O}(\mathbf{q}_+, \mathbf{q}_-) = -\mathcal{O}(-\mathbf{q}_-, -\mathbf{q}_+)$ depending on the momenta of the charged particles in the final state. A detailed analysis with simple observables of this form has been performed in ref. [109] for the channels (6.1). Repeating this analysis at $\sqrt{s} = 190$ GeV and assuming an integrated luminosity of $500\ (pb)^{-1}$ we find that with these observables one can test the real parts of the weak and EDM dipole form factors with the following accuracies:

$$\delta\mathrm{Re}\, d_\tau^Z(\sqrt{s} = 190 \text{ GeV}) \quad \simeq \quad 3.1 \times 10^{-17} ecm \quad (2\sigma), \tag{6.2}$$
$$\delta\mathrm{Re}\, d_\tau^\gamma(\sqrt{s} = 190 \text{ GeV}) \quad \simeq \quad 5.1 \times 10^{-16} ecm \quad (2\sigma). \tag{6.3}$$

The considerably smaller statistics at LEP2 is only partially compensated by the increase in sensitivity to the form factors at higher c.m. energies.

However, one can do better. For the channels with only two neutrinos in the final state the tau direction of flight can be reconstructed up to a two-fold ambiguity. This ambiguity can in principle be resolved [110]; its resolution is, however, not absolutely necessary (for details, see ref. [104]). In the following we assume that the $\tau^\pm$ directions of flight are known. The τ^+ momentum direction in the overall c.m. frame is denoted by $\hat{\mathbf{k}}$. Then one finds that the following CP- and T-odd observables involving the $\tau^\pm$ spins ($\sigma_{i\pm}$ are the Pauli matrices with $\pm$ refering to the respective spin spaces, and $\hat{\mathbf{p}}$ is the direction of the incoming positron),

$$\mathcal{O}_1 \quad = \quad (\hat{\mathbf{p}} \times \hat{\mathbf{k}}) \cdot (\boldsymbol{\sigma}_+ - \boldsymbol{\sigma}_-), \tag{6.4}$$
$$\mathcal{O}_2 \quad = \quad \hat{\mathbf{k}} \cdot \boldsymbol{\sigma}_+ (\hat{\mathbf{p}} \times \hat{\mathbf{k}}) \cdot \boldsymbol{\sigma}_- - \hat{\mathbf{k}} \cdot \boldsymbol{\sigma}_- (\hat{\mathbf{p}} \times \hat{\mathbf{k}}) \cdot \boldsymbol{\sigma}_+, \tag{6.5}$$

are suitable for tracing the above form factors. We find that $\mathcal{O}_1$ is mainly sensitive to $\mathrm{Re}\, d_\tau^Z$, whereas $\mathcal{O}_2$ is mainly sensitive to $\mathrm{Re}\, d_\tau^\gamma$. Needless to say the tau spins are analysed by the

decay distributions of the charged prongs. (The distributions are given, for example, in ref. [109].) Moreover one can use optimized observables $\mathcal{O}_i \to \mathcal{O}_i^{opt}$ with maximal signal-to-noise ratio. At $\sqrt{s}$=190 GeV and with an integrated luminosity of 500 $(pb)^{-1}$ we find that with these observables, using the channels $A, B = \pi, \rho, a_1$, the following sensitivities can be reached:

$$\delta \mathrm{Re}\, d_\tau^Z(\sqrt{s} = 190\mathrm{GeV}) \quad \simeq \quad 2.7 \times 10^{-17} ecm \quad (2\sigma), \tag{6.6}$$

$$\delta \mathrm{Re}\, d_\tau^\gamma(\sqrt{s} = 190\mathrm{GeV}) \quad \simeq \quad 4.9 \times 10^{-17} ecm \quad (2\sigma). \tag{6.7}$$

We mention that one can find spin-momentum observables whose expectation values are proportional to the imaginary parts of the form factors.

Also of interest are searches of non-standard CP violation in the reactions $e^+ e^- \to b\bar{b}\ gluon(s) \to 3jets$. (For details, see ref. [111].) Here one would be sensitive to CP-violating but chirality-conserving form factors of the $\gamma b\bar{b}g$ and $Zb\bar{b}g$ vertices. However, due to the small number of events at LEP2, assuming an integrated luminosity of 500 $(pb)^{-1}$, the sensitivity to these form factors at $\sqrt{s} = 190$ GeV is smaller by a factor of four as compared to the sensitivity at the Z peak.

In conclusion, measurements of CP-odd correlations in tau pair production at LEP2 would test the weak dipole form factor d_τ^Z with a sensitivity slightly below the accuracy reached at LEP1, but at higher energy. In addition, one can probe the EDM form factor d_τ^γ directly, and with better sensitivity than the direct test at LEP1. Essentially the same conclusions are reached at $\sqrt{s} = 175$ GeV assuming the same integrated luminosity.

References

[1] Y. Gol'fand and E. Likhtam, *JETP Lett.* **13** (1971) 323;
D. Volkov and V. Akulov, *Phys. Lett.* **B46** (1973) 109;
J. Wess and B. Zumino, *Nucl. Phys.* **B70** (1974) 39.

[2] J. Wess and J. Bagger, *Supersymmetry and Supergravity* (Princeton University Press,1983);
H.P. Nilles, *Phys. Rep.* **110** (1984) 1;
H.E. Haber and G.L. Kane, *Phys. Rep.* **117** (1985) 75;
R. Barbieri, *Riv. Nuovo Cim.* **11** (1988) 1;
R. Arnowitt, A. Chamseddine, and P. Nath, *Applied N=1 Supergravity* (World Scientific, 1984);
P. West, *Introduction to Supersymmetry and Supergravity* (World Scientific, 1986);
R.N. Mohapatra, *Unification and Supersymmetry* (Springer-Verlag, 1986).

[3] K. Wilson, as quoted by L. Susskind, *Phys. Rev.* **D20** (1979) 2619;
G. 't Hooft, in *Recent Developments in Gauge Theories*, ed. by G. 't Hooft *et al.* (Plenum Press, 1980);
L. Maiani, Proc. Summer School of Gif-sur-Yvette (1980);
M. Veltman, *Acta Phys. Polon.* **B12** (1981) 437.

[4] J. Ellis, K. Enqvist, D.V. Nanopoulos, and F. Zwirner, *Mod. Phys. Lett.* **A1** (1986) 57;
R. Barbieri and G.F. Giudice, *Nucl. Phys.* **B306** (1988) 63;
S. Dimopoulos and G.F. Giudice, *Phys. Lett.* **B357** (1995) 573.

[5] J. Ellis, J.S. Hagelin, D.V. Nanopoulos, K. Olive, and M. Srednicki, *Nucl. Phys.* **B238** (1984) 453.

[6] Review of particle properties, L. Montanet et al., *Phys. Rev.* **D50** (1994) 1173.

[7] OPAL Collaboration, R. Akers *et al.*, *Phys. Lett.* **B337** (1994) 207.

[8] ALEPH Collaboration, Contribution #0416, International Europhysics Conference on High Energy Physics, Brussels, Belgium, 27 July - 2 August (1995).

[9] M. Acciarri et al., L3 Coll., *Phys. Lett.* **B350** (1995) 109.

[10] J. Hauser, for the CDF Coll., FERMILAB-CONF-95/172-E, to appear in the Proceedings of the 10th Topical Workshop on Proton-Antiproton Collider Physics, Batavia, IL, May 9-13 1995;
DØ Coll., contribution DØ #434. presented at the International Europhysics Conference on High Energy Physics, Brussels, Belgium, 27 July - 2 August (1995).

[11] The LEP Electroweak Working Group, CERN preprint LEPEWWG/95-02.

[12] G. Altarelli and R. Barbieri, *Phys. Lett.* **B253** (1991) 161;
G. Altarelli, R. Barbieri, and S. Jadach, *Nucl. Phys.* **B369** (1992) 3.

[13] J. Ellis, G.L. Fogli, E. Lisi preprint CERN–TH/95–202, BARI–TH/211–95;
P.H. Chankowski and S.Pokorski *Phys. Lett.* **B356** (1995) 307 and hep-ph/9509207;
J. Ellis, G.L. Fogli, E. Lisi *Phys. Lett.* **B292** (1992) 427, *Phys. Lett.* **B318** (1993) 375, *Phys. Lett.* **B324** (1994) 173, *Phys. Lett.* **B333** (1994) 118.

[14] J. Erler and P. Langacker, *Phys. Rev.* **D52** (1995) 441.

[15] G. Altarelli, R. Barbieri, and F. Caravaglios *Nucl. Phys.* **B405** (1993) 3, *Phys. Lett.* **314B** (1993) 357, *Phys. Lett.* **349** (1995) 145.

[16] P.H. Chankowski and S. Pokorski preprint MPI-PTh/95-49
hep-ph/9505308, *Phys. Lett.* **B** in press;
P.H. Chankowski talk at the International Europhysics Conference on High Energy Physics, Brussels, 27 July – 2 August, 1995, to appear in the Proceedings.

[17] A. Olchevski, plenary talk at the International Europhysics Conference on High Energy Physics, Brussels, 27 July – 2 August, 1995, to appear in the Proceedings.

[18] M. Boulware and D. Finnell, *Phys. Rev.* **D44** (1991) 2054;
J. Rosiek, *Phys. Lett.* **B252** (1990) 135;
A.Denner et al., *Z. Phys.* **C51** (1991) 695.

[19] D. Garcia, A. Jimenéz and J. Solà, *Phys. Lett.* **347B** (1995) 309, E **351B** (1995) 602.

[20] G.L. Kane R.G. Stuart and J.D. Wells, *Phys. Lett.* **B338** (1994) 219;
J.D. Wells and G.L. Kane, preprint SLAC-PUB-7038 (1995).

[21] S. Bertolini, F. Borzumati, A. Masiero and G. Ridolfi, *Nucl. Phys.* **B353** (1991) 591;
R. Barbieri and G.F. Giudice, *Phys. Lett.* **309B** (1993) 86;
A. Buras, M. Misiak, M. Münz and S. Pokorski, *Nucl. Phys.* **B424** (1994) 376.

[22] P. Krawczyk, S. Pokorski *Phys. Rev. Lett.* **60** (1988) 182,
G. Isidori *Phys. Lett.* **298B** (1993) 409.

[23] M. Carena, S. Pokorski, and C.E.M. Wagner *Nucl. Phys.* **B406** (1994) 59;
W. Bardeen, M. Carena, S. Pokorski,and C.E.M. Wagner, *Phys. Lett.* **B320** (1994) 110.

[24] M. Olechowski and S. Pokorski, *Phys. Lett.* **B214** (1988) 393;
G.F. Giudice and G. Ridolfi, *Z. Phys.* **C41** (1988) 447;
B. Ananhtarayan, G. Lazarides and Q. Shafi, *Phys. Rev.* **D44** (1991) 1613;
S. Dimopoulos, L.J. Hall, and S. Raby, *Phys. Rev. Lett.* **68** (1992) 1984, *Phys. Rev.* **D45** (1992) 4192.

[25] M. Olechowski and S. Pokorski, *Phys. Lett.* **344B** (1995) 201.

[26] See for instance:
J.L. Feng and M.J. Strassler, *Phys. Rev.* **D51** (1995) 4661;
A. Bartl, H. Fraas, W. Majerotto, and B. Mösslacher, *Z. Phys.* **C55** (1992) 257, and references therein.

[27] J.-F. Grivaz (ALEPH), *Prospects for Supersymmetry Discoveries at Future e^+e^- Colliders*, in the Proceedings of the Workshop "Properties of Supersymmetric Particles", Erice, Italy, 1992;
P. Rebecchi (DELPHI), presentation at the May Meeting of the LEP2 Workshop, "New Particles" subgroup;
S. Navas (DELPHI), presentation at the November meeting;
A. Trombini (DELPHI), private communication;
S. Rosier (L3), L3 Note 1863, in preparation;
S. Komamiya (OPAL), presentation at the September meeting;
R. Van Kooten (OPAL), private communication.

[28] T. Sjöstrand and M. Bengtsson, Comput. Phys. Commun. 43 (1987) 367;
T.Sjöstrand,in: Z Physics at LEP 1, eds. G. Altarelli et al., CERN Report CERN-89-08, Vol. 3 (1989) 143;
T. Sjöstrand, Comput. Phys. Commun. 82 (1994) 74.

[29] TWOGAM, S. Nova, A. Olshevski, and T. Todorov, DELPHI 90-35 PROG 152.

[30] See the "Event Generators for New Physics" Chapter, in vol II of this Report.

[31] H. Baer, M. Brhlik, R. Munroe and X. Tata, *Phys. Rev.* **D52** (1995) 5031.

[32] F. Nessi-Tedaldi, "Monte Carlo study of selectron searches with L3 at LEP2", L3 Internal Note 1576 (1995), and private communication.

[33] R. Becker, PITHA 93/27, (Aachen, 1993).

[34] C.Vander Velde, IIHE report, ULB/VUB-Brussels, "Monte Carlo study of slepton searches with DELPHI at LEP2", in preparation.

[35] L.Favart, presentation at the September 27 1995 Meeting of the LEP2 workshop, "New Particles" subgroup and private communication.

[36] Koji Yoshimura, presentation at the November 1 1995 Meeting of the LEP2 workshop, "New Particles" subgroup and private communication.

[37] A. Bartl, W. Majerotto, and W. Porod, *Z. Phys.* **C64** (1994) 499.

[38] M. Drees and K. Hikasa, *Phys. Lett.* **B252** (1990) 127.

[39] W. Beenakker, R, Hoepker, P.M.Zerwas, *Phys. Lett.* **B349** (1995) 463.

[40] K. Hikasa and M. Kobayashi, *Phys. Rev.* **D36** (1987) 724.

[41] A. Sopczak, L3 Note 1860 (1995)

[42] S. Asai, S. Komamiya and S. Orito, UT-ICEPP 95-10 (1995)

[43] M. Besançon, DELPHI Note, in preparation.

[44] D. Claes, for the DØ Coll., contribution DØ #435. presented at the International Europhysics Conference on High Energy Physics, Brussels, Belgium, 27 July - 2 August (1995).

[45] S. Ambrosanio and B. Mele, *Phys. Rev.* **D52** (1995) 3900.

[46] S. Ambrosanio and B. Mele, "Neutralino Decays in the Minimal Supersymmetric Standard Model", Preprint ROME1-1095/95, hep-ph/9508237, August 1995, to appear in *Phys. Rev.* D.

[47] S. Ambrosanio, M. Carena, B. Mele, C. E. M. Wagner, Preprint CERN-TH/95-286, ROME1-1121/95, hep-ph/9511259, (1995), submitted for publication in *Phys. Lett.* B.

[48] G.F. Giudice and A. Pomarol, preprint CERN-TH/95-337.

[49] S. Ambrosanio, B. Mele, G. Montagna, O. Nicrosini, F. Piccinini, preprint FNT/T-95/32, ROME1-1126/95 (1995).

[50] M. Felcini and J. Toth, L3 Note 1874, Nov 1995.

[51] H.-P. Nilles, M. Srednicki, and D. Wyler, *Phys. Lett.* **B120** (1983) 346;
J.-P. Derendinger and C.A. Savoy, *Nucl. Phys.* **B237** (1984) 307;
J. Ellis, J.F. Gunion, H.E. Haber, L. Roszkowski, and F. Zwirner, *Phys. Rev.* **D39** (1989) 844;
M. Drees, *Int. Jour. Mod. Phys.* **A4** (1989) 3635;
U. Ellwanger, M. Rausch de Traubenberg, and C. A. Savoy, *Phys. Lett.* **B315** (1993) 331;
T. Elliott, S.F. King, and P.L. White, *Phys. Lett.* **B351** (1995) 213.

[52] F. Franke, H. Fraas and A. Bartl, *Phys. Lett.* **B336** (1994) 415;
F. Franke and H. Fraas, *Phys. Lett.* **B353** (1995) 234.

[53] F. Franke and H. Fraas, WUE-ITP-95-021, hep-ph/9511275.

[54] F. Zwirner, *Phys. Lett.* **132B** (1983) 103;
L.J. Hall and M. Suzuki, *Nucl. Phys.* **B231** (1984) 419;
L. Ibanez and G.G. Ross, *Nucl. Phys.* **B368** (1992) 3.

[55] H. Dreiner and A. Chamseddine, ETH-TH-95-04, hep-ph/9504337.

[56] H. Dreiner and G.G. Ross, *Nucl. Phys.* **B365** (1991) 597.

[57] R.M. Godbole, P. Roy, and X. Tata, *Nucl. Phys.* **B401** (1993) 67;
V. Barger, W.-Y. Keung, and R.J.N. Phillips, *Phys. Lett.* **B356** (1995) 546.

[58] H. Dreiner and P. Morawitz, *Nucl. Phys.* **B428** (1994) 31.

[59] V. Barger, G.F. Giudice, and T. Han, *Phys. Rev.* **D40** (1989) 2987.

[60] H. Baer, F. Paige, S. Protopopescu and X. Tata, in *Proceedings of the Workshop on Physics at Current Accelerators and Supercolliders*, ed. J. Hewett, A. White and D. Zeppenfeld, (Argonne National Laboratory, 1993); see also contribution by H. Baer, F. Paige and X. Tata in event generators section.

[61] HELAS: HELicity Amplitude Subroutines for Feynman Diagram Evaluations, H. Murayama, I. Watanabe and K. Hagiwara, KEK-91-11 (1992).

[62] J.C. Pati and A. Salam, *Phys. Rev.* **D10** (1974) 275;
R.N. Mohapatra and J.C. Pati, *Phys. Rev.* **D11** (1975) 366,2588;
G. Senjanović and R.N. Mohapatra, *Phys. Rev.* **D12** (1975) 1502.

[63] J. Hewett and T. G. Rizzo, *Phys. Rep.* **183** (1989) 193;
J. Maalampi and M. Roos, *Phys. Rep.* **186** (1990) 53;
W. Buchmüller and C. Greub, *Nucl. Phys.* **B363** (1991) 345; *Nucl. Phys.* **B381** (1992) 109.

[64] Proceedings of the International Symposium on the 4th Family of Quarks and Leptons, Santa Monica (1987), Ann. New York Accademy of Science, 518 (eds. D.B. Cline and A. Soni).

[65] M. Chanowitz, M. Furman and I. Hinchliffe, *Phys. Lett.* **B78** (1978) 285;
M. Drees, *Nucl. Phys.* **298** (1988) 333;
F. Csikor and I. Montvay, *Phys. Lett.* **B231** (1990) 503.

[66] K. Hagiwara, S. Komamiya and D. Zeppenfeld, *Z. Phys.* **C29** (1985) 115.

[67] A. Djouadi *et. al.*, SLAC-PUB-95-6772 (To appear in *Electroweak Symmetry Breaking and Beyond the Standard Model*, eds. T. Barklow, S. Dawson, H.E. Haber and S. Siegrist, World Scientific.)

[68] B. Mukhopadhyaya and D.P. Roy, *Phys. Rev.* **D48** (1993) 2105.

[69] E. Nardi, E. Roulet, and D. Tommasini, *Phys. Lett.* **B344** (1995) 225;
G. Bhattacharyya et al., *Mod. Phys. Lett.* **A6** (1991) 2921;
G. Bhattacharyya, *Phys. Lett.* **B331** (1994) 143.

[70] P. Langacker, Proc. of SUSY-95, hep-ph/9511207.

[71] J.J. van der Bij and F. Hoogeveen, *Nucl. Phys.* **B283** (1987) 477;
M. Consoli, W. Hollik and F. Jegerlehner, *Phys. Lett.* **B227** (1989) 167;
Also see A. Sirlin, hep-ph/9411363 (To appear in '*Reports of the Working Group on Precision Calculations for the Z resonance*') and the references therein.

[72] S. Shevchenko and A. Shvorob, L3 internal note (in preparation).

[73] G. Bhattacharyya and D. Choudhury, CERN preprint CERN-TH/95-306.

[74] A. Djouadi, *Z. Phys.* **C63** (1994) 317;
A. Djouadi and G. Azuelos, *Z. Phys.* **C63** (1994) 327.

[75] R. Tafirout and G. Azuelos, OPAL Internal note.

[76] F. Boudjema, A. Djouadi and J.L. Kneur, *Z. Phys.* **C57** (1993) 425.

[77] M. Martinez, and R. Miquel, *Phys. Lett.* **B302** (1993) 108.

[78] ALEPH Collaboration, *Phys. Rep.* **216** (1992) 1.

[79] A. Litke, Experiments with Electron-Positron Colliding beams, PhD Thesis, Harvard University (1970).

[80] J. Pati and A. Salam, *Phys. Rev.* **D10** (1974) 275;
P. Langacker, *Phys. Rep.* **72** (1981) 185;
B. Schrempp and F. Schrempp, *Phys. Lett.* **B153** (1985) 101;
J.L. Hewett and T.G. Rizzo, *Phys. Rep.* **193** (1989) 193;
P.H. Frampton, *Mod. Phys. Lett.* **A7** (1992) 559;

[81] W. Buchmüller, R. Rückl and D. Wyler, *Phys. Lett.* **B191** (1987) 442.

[82] J. Blümlein and R. Rückl, *Phys. Lett.* **B304** (1993) 337.

[83] O. Shanker, *Nucl. Phys.* **B204** (1982) 375;
W. Buchmüller and D. Wyler, *Phys. Lett.* **B177** (1986) 377;
J.L. Hewett and T.G. Rizzo, *Phys. Rev.* **D36** (1987) 3367;
M. Leurer, *Phys. Rev.* **D49** (1994) 333;
S. Davidson, D. Bailey and A. Campbell, *Z. Phys.* **C61** (1994) 613.

[84] J.K. Mizukoshi, O.J.P. Eboli and M.C. Gonzalez-Garcia, CERN-TH.7508/94 (1994);
G. Bhattacharyya, J. Ellis and K. Sridhar, CERN-TH.7280/94 (1994).

[85] H1 Collaboration, T. Ahmed et. al., *Z. Phys.* **C64** (1994) 545; DESY 95-079.

[86] L3 Collaboration, B. Adeva et. al., *Phys. Lett.* **B261** (1991) 169;
OPAL Collaboration, G. Alexander et. al., *Phys. Lett.* **B263** (1991) 123;
DELPHI Collaboration, P. Abreu et. al., *Phys. Lett.* **B316** (1993) 620;
ALEPH Collaboration, D. Decamp et al., CERN PPE/91-149.

[87] D0 Collaboration, S. Abachi et.al., *Phys. Rev. Lett.* **72** (1994) 965.

[88] CDF Collaboration, F. Abe et. al., *Phys. Rev. Lett.* **75** (1995) 1012.

[89] L3 Collaboration, O. Adriani et al., CERN-PPE/93-31 (1993).

[90] S. Weinberg, *Phys. Rev.* **D19** (1979) 1277;
L. Susskind, *Phys. Rev.* **D20** (1979) 2619;
E. Farhi and L. Susskind, *Phys. Rep.* **74** (1981) 277.

[91] For reviews, see M. Chanowitz, *Annu. Rev. Nucl. Part. Sci.* **38** (1988) 323;
T. Appelquist, Lectures given at Mexican School of Particles and Fields, Mexico City, December 1990 (preprint YCTP-P23-91).

[92] R. Casalbuoni, S. De Curtis, D. Dominici and R. Gatto, *Phys. Lett.* **B155** (1985) 95; *Nucl. Phys.* **B282** (1987) 235;
R. Casalbuoni, S. De Curtis, D. Dominici, F. Feruglio and R. Gatto, *Int. Jour. Mod. Phys.* **A4** (1989) 1065.

[93] R. Casalbuoni, A. Deandrea, S. De Curtis, D. Dominici, F. Feruglio, R. Gatto and M. Grazzini, *Phys. Lett.* **B349** (1995) 533;
R. Casalbuoni, A. Deandrea, S. De Curtis, D. Dominici, R. Gatto and M. Grazzini, UGVA-DPT 1995/10-906 (hep-ph/9510431), (1995).

[94] F. Caravaglios, talk given at the International Europhysics Conference on High Energy Physics, Brussels, 27 July – 2 August, 1995, to appear in the Proceedings.

[95] F. Feruglio, A. Masiero, S. Rigolin, R. Strocchi, *Phys. Lett.* **B355** (1995) 329.

[96] R. Barbieri, F. Caravaglios and M. Frigeni, *Phys. Lett.* **B279** (1992) 169.

[97] K.J.F. Gaemers, G.J. Gounaris, *Z. Phys.* **C1** (1979) 259;
K. Hagiwara, K. Hikasa, R. Peccei and D. Zeppenfeld, *Nucl. Phys.* **B282** (1987) 253.

[98] E.N. Argyres, C.G. Papadopoulos, *Phys. Lett.* **B263** (1991) 298;
E.N. Argyres, G. Katsilieris, A.B. Lahanas, C.G. Papadopoulos, V.C. Spanos, *Nucl. Phys.* **B391** (1993) 23;
J. Fleischer, J.L. Kneur, K. Kolodziej, M. Kuroda, D. Schildknecht, *Nucl. Phys.* **B378** (1992) 443, *Nucl. Phys.* **B426** (1994) 246.

[99] M. Bilenky, J.L. Kneur, F.M. Renard, D. Schildknecht, *Nucl. Phys.* **B409** (1993) 22; *Nucl. Phys.* **B419** (1994) 240.

[100] A.B. Lahanas, V.C. Spanos, *Phys. Lett.* **B334** (1994) 378; hep-ph 9504340;
A. Culatti, *Z. Phys.* **C65** (1995) 537.

[101] W. Bernreuther, G. Botz, O. Nachtmann, and P. Overmann, *Z. Phys.* **C52** (1991) 567.

[102] Triple Gauge Boson Couplings, in this report.

[103] W. Bernreuther, A. Brandenburg and P. Overmann, to be published.

[104] R. Akers et al. (OPAL collab.), *Z. Phys.* **C66** (1995) 31.

[105] D. Buskulic et al. (ALEPH collab.), *Phys. Lett.* **B346** (1995) 371.

[106] A. Stahl, *Nucl. Phys* **B40** (Proc. Suppl.) (1995) 505.

[107] A. Venturi, in Proc. of the XXVII Int. Conf. on High Energy Physics, ed. by P.J. Bussey and I.G. Knowles, Bristol (1995) p. 771.

[108] R. Escribano and E. Masso, *Phys. Lett.* **B301** (1993) 419.

[109] W. Bernreuther, O. Nachtmann and P. Overmann, *Phys. Rev.* **D48** (1993) 78.

[110] J.H. Kühn, *Phys. Lett.* **B313** (1993) 458.

[111] J. Körner et al., *Z. Phys.* **C49** (1991) 447;
W. Bernreuther et al., *Z. Phys.* **C68** (1995) 73.